

2014

Monitoring conterminous United States (CONUS) land cover change with Web-Enabled Landsat Data (WELD)

M C. Hansen

University of Maryland, College Park, mhansen@umd.edu

A. Egorov

South Dakota State University, Alexey.Egorov@sdstate.edu

P V. Potapov

University of Maryland, College Park

S V. Stehman


State University of New York

A Tyukavina

University of Maryland, College Park

See next page for additional authors

Follow this and additional works at: <http://digitalcommons.unl.edu/usgsstaffpub>

 Part of the [Earth Sciences Commons](#), [Environmental Sciences Commons](#), and the [Oceanography and Atmospheric Sciences and Meteorology Commons](#)

Hansen, M C.; Egorov, A.; Potapov, P V.; Stehman, S V.; Tyukavina, A.; Turubanova, S A.; Roy, D. P.; Goetz, S J.; Loveland, T R.; Ju, J.; Kommareddy, A.; Kovalsky, V.; Forsyth, C; and Bents, T, "Monitoring conterminous United States (CONUS) land cover change with Web-Enabled Landsat Data (WELD)" (2014). *USGS Staff -- Published Research*. 854.
<http://digitalcommons.unl.edu/usgsstaffpub/854>

This Article is brought to you for free and open access by the US Geological Survey at DigitalCommons@University of Nebraska - Lincoln. It has been accepted for inclusion in USGS Staff -- Published Research by an authorized administrator of DigitalCommons@University of Nebraska - Lincoln.

Authors

M C. Hansen, A. Egorov, P V. Potapov, S V. Stehman, A Tyukavina, S A. Turubanova, D. P. Roy, S J. Goetz, T R. Loveland, J Ju, A. Kommareddy, V. Kovalsky, C Forsyth, and T Bents



Monitoring conterminous United States (CONUS) land cover change with Web-Enabled Landsat Data (WELD)



M.C. Hansen ^{a,*}, A. Egorov ^b, P.V. Potapov ^a, S.V. Stehman ^c, A. Tyukavina ^a, S.A. Turubanova ^a, D.P. Roy ^b, S.J. Goetz ^d, T.R. Loveland ^e, J. Ju ^f, A. Kommareddy ^b, V. Kovalsky ^b, C. Forsyth ^b, T. Bents ^g

^a University of Maryland, College Park, MD, United States

^b South Dakota State University, Brookings, SD, United States

^c State University of New York, Syracuse, NY, United States

^d Woods Hole Research Center, Falmouth, MA, United States

^e USGS EROS, Sioux Falls, SD, United States

^f NASA GSFC, Greenbelt, MD, United States

^g University of Kansas, Lawrence, KS, United States

ARTICLE INFO

Article history:

Received 1 January 2013

Received in revised form 13 August 2013

Accepted 14 August 2013

Available online 11 October 2013

Keywords:

Change detection

Land cover

Landsat

Large area mapping

Validation

ABSTRACT

Forest cover loss and bare ground gain from 2006 to 2010 for the conterminous United States (CONUS) were quantified at a 30 m spatial resolution using Web-Enabled Landsat Data available from the USGS Center for Earth Resources Observation and Science (EROS) (<http://landsat.usgs.gov/WELD.php>). The approach related multi-temporal WELD metrics and expert-derived training data for forest cover loss and bare ground gain through a decision tree classification algorithm. Forest cover loss was reported at state and ecoregional scales, and the identification of core forests' absent of change was made and verified using LiDAR data from the GLAS (Geoscience Laser Altimetry System) instrument. Bare ground gain correlated with population change for large metropolitan statistical areas (MSAs) outside of desert or semi-desert environments. GoogleEarth™ time-series images were used to validate the products. Mapped forest cover loss totaled 53,084 km² and was found to be depicted conservatively, with a user's accuracy of 78% and a producer's accuracy of 68%. Excluding errors of adjacency, user's and producer's accuracies rose to 93% and 89%, respectively. Mapped bare ground gain equaled 5974 km² and nearly matched the estimated area from the reference (GoogleEarth™) classification; however, user's (42%) and producer's (49%) accuracies were much less than those of the forest cover loss product. Excluding errors of adjacency, user's and producer's accuracies rose to 62% and 75%, respectively. Compared to recent 2001–2006 USGS National Land Cover Database validation data for forest loss (82% and 30% for respective user's and producer's accuracies) and urban gain (72% and 18% for respective user's and producer's accuracies), results using a single CONUS-scale model with WELD data are promising and point to the potential for national-scale operational mapping of key land cover transitions. However, validation results highlighted limitations, some of which can be addressed by improving training data, creating a more robust image feature space, adding contemporaneous Landsat 5 data to the inputs, and modifying definition sets to account for differences in temporal and spatial observational scales. The presented land cover extent and change data are available via the official WELD website (ftp://weldftp.cr.usgs.gov/CONUS_5Y_LandCover/ftp://weldftp.cr.usgs.gov/CONUS_5Y_LandCover/).

© 2013 Elsevier Inc. All rights reserved.

1. Introduction

Quantifying global change via earth observation data is a pressing need given the changing state of global climate, biodiversity, food and fiber demand, and other critical environmental/ecosystem services. Land cover has been recognized as a key measure of global environmental change by the United Nations Framework Convention on Climate Change (UNFCCC) and as an essential climate variable by the Global Climate and

Global Terrestrial Observing Systems (GCOS and GTOS). Land cover change also informs all nine societal benefit areas of the Group on Earth Observations (GEO). As such, approaches to systematically monitor land cover change are needed to better quantify earth system dynamics. With the opening of the United States Geological Survey's (USGS) Landsat data archive (Woodcock et al., 2008; Wulder, Masek, Cohen, Loveland, & Woodcock, 2012) and the newly launched Landsat Data Continuity Mission (LDCM), access to a record of historical and future global land change is assured (Irons & Loveland, 2013). Along with the liberalization of the Landsat data policy, there are also new high-performance computing capabilities that enable the systematic processing of high

* Corresponding author.

E-mail address: mhansen@umd.edu (M.C. Hansen).

volumes of imagery in the support of land cover extent and change characterization. The confluence of these three factors – information need, data access and computing power – points to a realistic expectation of quantifying global land change.

Historically, large area land change investigations using Landsat data have been based on approaches in which the inputs are individually characterized at the scene or ecozone level (Cacetta et al., 2007; Harper, Steininger, Tucker, Juhn, & Hawkins, 2007; INPE, 2010; Killeen et al., 2007; Leimgruber et al., 2005; Xian & Homer, 2010; Xian, Homer, & Fry, 2009). Recent global land cover extent and change mapping methods employ the per scene characterization approach (Gong et al., 2013; Sexton et al., 2013a; Townshend et al., 2012). The individual characterizations are subsequently stitched together to derive a large area land cover map product. Another option is to apply algorithms at national to continental scales (Hansen et al., 2011). While this is common practice with coarse spatial resolution imagery such as MODIS (Friedl et al., 2002; Hansen et al., 2003), it is not often performed using Landsat imagery, especially for change estimation. Masek et al. (2008) applied a standard disturbance index for North America using such an approach. The study presented here does so as well, and is an extension of previous national-scale forest cover loss characterizations for Indonesia, European Russia and the Democratic Republic of the Congo (Broich et al., 2011; Potapov et al. 2012a; Potapov et al., 2012b).

Methods and results presented here employ data from the NASA-funded Web-Enabled Landsat Data (WELD) project, which has implemented large volume pre-processing of Landsat 7 Enhanced Thematic Mapper Plus (ETM+) scan-line corrector off (SLC-off) data, to map land cover extent and change. WELD data consist of 30 m spatial resolution mosaicked and temporally composited time-series data sets for the conterminous United States (CONUS) and Alaska (<http://landsat.usgs.gov/WELD.php>) (Roy et al., 2010). Data products such as WELD will facilitate future large area land cover analyses and allow researchers and operational agencies to move from national to global scales, mimicking and improving upon current land cover products derived more commonly with coarse resolution data (Friedl et al., 2002; Hansen et al., 2003).

During the 2010 GEO ministerial summit in Beijing, the U.S. Department of the Interior (DOI) announced an initiative to develop a global land cover change monitoring system based on Landsat imagery (Department of Interior, 2010). The U.S. Geological Survey is leading this initiative and has partnered with the University of Maryland (UMD) and South Dakota State University (SDSU) for system and methodological research and development. In order to be efficient, consistent, and timely, scene-based Landsat inputs are not practical and so the USGS-UMD-SDSU team is testing the feasibility for using WELD as a foundation for land-cover monitoring. The grand challenge in global land cover mapping is to be locally relevant and globally consistent. Early research reported by Hansen et al. (2011) showed that the WELD configuration based on Landsat 7 data was sufficient for producing land cover characterizations at continental scales that are internally consistent while still retaining local spatial and thematic detail. The research reported here provides additional evidence of the feasibility for using the seamless WELD time series to quantify large area land cover properties and track land change as envisioned for the GEO global land cover initiative.

This paper presents the derivation of land cover change products for the CONUS from 2006 to 2010 for tree cover loss and bare ground gain. The method employs the WELD Vegetation Continuous Fields of percent tree cover and percent bare ground (Hansen et al., 2003, 2011) as a reference in the quantification of land cover change. A supervised learning method is employed where change is directly trained upon and related to a set of multi-temporal image metrics derived from WELD weekly growing season mosaics. Results, including per pixel forest cover loss, bare ground gain and estimated date of change, are presented. Gross forest cover loss is defined as a stand-replacement disturbance at the

30 m Landsat pixel scale, and includes mechanical clearing, fire, storm and disease-related causes of forest stand-replacement disturbance. Forest cover loss does not include selective logging dynamics. Bare ground gain is defined as complete permanent or semi-permanent removal of vegetative cover at the 30 m Landsat pixel scale. Bare ground gain consists of expansion of impervious surface due to commercial, residential and infrastructure development, as well as mining and denudation of vegetation due to landslides, river meanders and other natural causes of bare ground exposure. Thematic outputs similar to bare ground gain include impervious surface (Goetz, Wright, Smith, Zinecker, & Schaub, 2003; Sexton et al., 2013b); however, for this study impervious surface gain is a subset of total bare ground gain. Bare ground gain does not include events such as agricultural fallows or land clearings that are ephemeral and followed by relatively rapid vegetation recovery. Value-added analyses include forest cover loss by ecoregion and bare ground gain by metropolitan statistical area.

2. Data

2.1. WELD data

The WELD data are generated from the USGS Level 1 terrain corrected (L1T) Landsat data. The Level 1T processing includes radiometric calibration and geometric correction using ground control chips and a digital elevation model to correct error due to local topographic relief. Reported geolocation error is less than 30 m for CONUS (Lee, Storey, Choate, & Hayes, 2004). Enhanced Thematic Mapper Plus (ETM+) L1T data are used to make WELD weekly, monthly, seasonal and annual composited mosaics (Roy et al., 2010). For this study, we used the WELD weekly mosaics. Each WELD mosaic defines at 30 m the top of atmosphere reflectance, brightness temperature, normalized difference vegetation index (NDVI), band saturation status, and cloud state information. Radiometrically corrected data such as WELD facilitate large area land cover mapping by minimizing remote sensing variations introduced by differences in sun–earth distance, solar geometry, and exoatmospheric solar irradiance arising from spectral band differences (Chander, Markham, & Helder, 2009). The WELD per-pixel temporal compositing approach uses criteria based on selecting from multiple ETM+ observations of the same pixel the observation that is not cloud contaminated or missing. If several observations meet this criterion, the observation with the maximum NDVI is chosen; for certain low vegetation covers, the observation with the maximum brightness temperature is selected. These criteria are modified based on the band saturation status, as NDVI and brightness temperature cannot be retrieved reliably from saturated pixels. The compositing approach is primarily driven by the maximum NDVI compositing criterion which preferentially selects the greenest dates (Holben, 1986; Roy, 2000).

For this research we used weekly CONUS WELD mosaics from April 15 through November 17 for 2006 to 2010 inclusive. Winter, late fall, and early spring data were not used to avoid phenological-related change and data poor times of year, particularly the winter and spring seasons which have fewer viable observations due to persistent cloud and snow (Ju & Roy, 2008). From the mosaics the top of atmosphere (TOA) reflectance of ETM+ bands 1 (0.45–0.515 μm), 2 (0.525–0.605 μm), 3 (0.63–0.69 μm), 4 (0.78–0.90 μm), 5 (1.55–1.75 μm), and 7 (2.09–2.35 μm) were used as inputs to feature space generation.

Temporal metrics were derived from these data on an annual and multi-year basis. Metrics have been shown to be a viable transformation of time-series data in quantifying land cover change, in particular forest cover. Their use in quantifying change began with coarse spatial resolution imagery in characterizing land cover (DeFries, Hansen, & Townshend, 1995; Reed et al., 1994) and forest cover change (Hansen & DeFries, 2004; Hansen et al., 2008; Hansen et al., 2010). Metrics have been shown to provide a generalized feature space that has advantages over time-sequential composite imagery in mapping large area (continental to global-scale) land cover (Hansen, Townshend, DeFries,

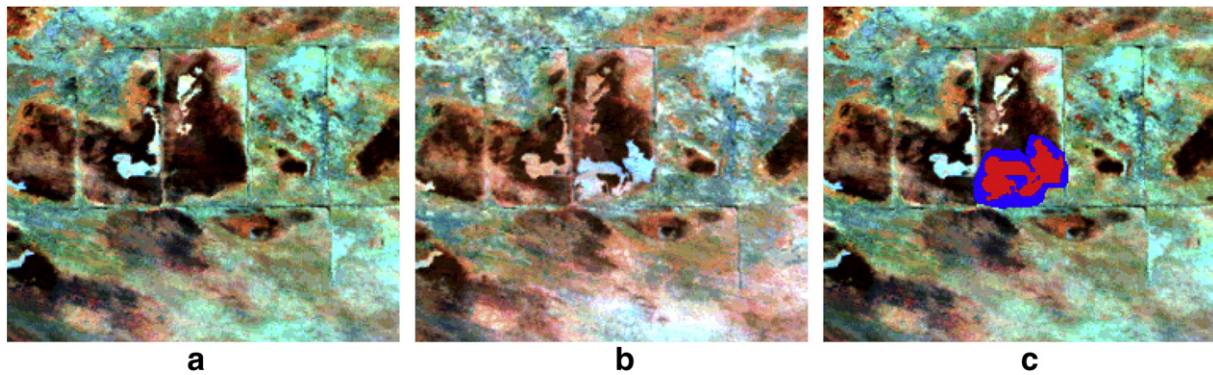


Fig. 1. Example training site from Minnesota where a) is median growing season image for 2006, b) is median growing season image for 2010, and c) is 2006 image with training sites for forest cover loss (red) and no forest cover loss (blue). Subset is centered on 48 20 43N, 94 57 24W and is 7 km by 5 km in extent. Strategy for training data delineation is outlined in Hansen (2012).

& Carroll, 2005). Metrics capture the salient features of vegetation phenology and land change without regard to specific time of year. For example, Chang, Hansen, Pittman, Dimiceli, and Carroll (2007) found a growing season NDVI amplitude most useful in identifying corn and soybean cover at the national scale using MODIS data. Broich et al. (2011) found Landsat-derived time-integrated metrics to be superior to bi-temporal change methods in mapping forest loss in Indonesia. Potapov et al. (2012b) also applied Landsat-derived metrics to characterize decadal-scale forest loss for the Democratic Republic of the Congo.

Unlike MODIS data, Landsat ETM+ data are characterized by highly unequal observation counts due to a varying Landsat acquisition strategy (Kovalskyy, V. and Roy, D.P., 2013). Further, the weekly WELD products have along scan stripes of missing data due to the Landsat 7 ETM+ scan line corrector that failed in 2003 and reduces the usable data in each ETM+ scene by about 22% (Markham, Storey, Williams, & Irons, 2004). For CONUS, where all possible acquisitions are made, SLC-off gaps and cloud cover result in variable land observation counts over time. Metrics, such as simple percentiles over a given interval, help normalize the feature space derived from such data. Metrics are different than strictly time-series sequential methods such as those of Huang et al. (2009) and Kennedy, Yang, and Cohen (2010). While some metrics can be time-sequential, such as regression per band against date, most are

statistical measures derived over a period of study without regard to sequential timing. A total of 139 multi-temporal image metrics were generated from the WELD weekly mosaics, including:

- 5-year percentiles per band totaling 30 metrics (5 percentiles of 10, 25, 50, 75 and 90% per each of 6 bands calculated from all inputs from 2006 to 2010)
- First and last year percentiles totaling 60 metrics (5 percentiles of 10, 25, 50, 75 and 90% per each of 6 bands calculated for single year inputs of 2006 and 2010)
- Multi-year percentile differences totaling 12 metrics (90% minus 10%, 75% minus 25% per each of 6 bands)
- First and last year percentile differences totaling 30 metrics (i.e. between 10 percentile value of the first and the last year, 25, etc., for a total of 5 difference values per each of 6 bands)
- Slopes of linear regression between band reflectance and time-sequential observation date, totaling 6 metrics
- Number of good observations metric.

2.2. Training data

Training data were derived from image interpretation methods, including on-screen delineation of change and no change categories.

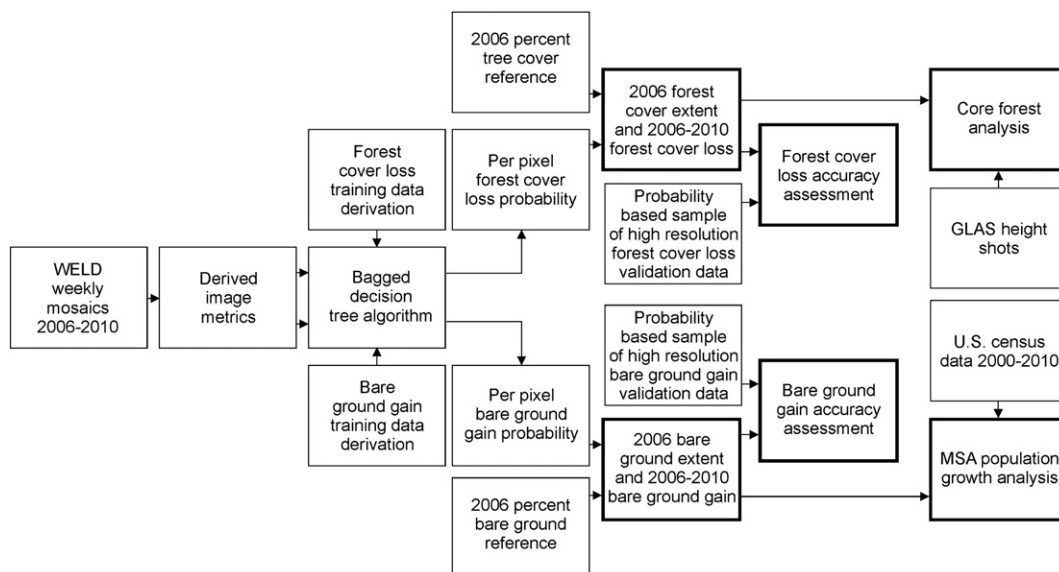


Fig. 2. Analysis flowchart.

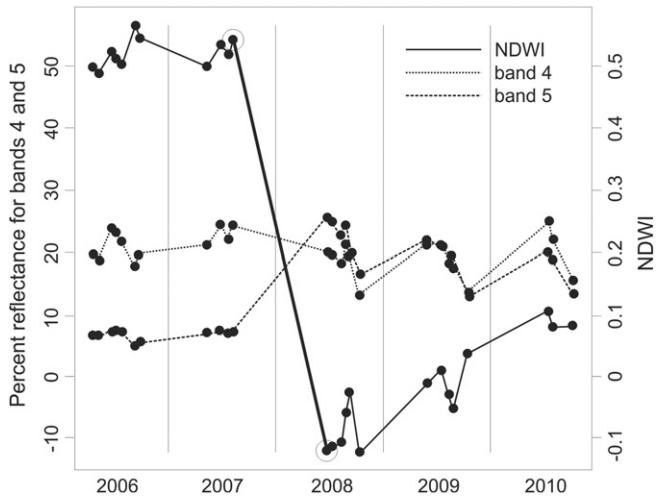


Fig. 3. Example forest cover loss pixel with time-series observations for growing season imagery from 2006 to 2010. The greatest drop in NDWI is shown by the circles and is used to assign the date using the first post-change observation. The location of this pixel is in the Pacific Northwest at 43 25 45N, 123 53 05W.

Various image composites, such as 2006 median 5–4–3 and 2010 median 5–4–3, as well as GoogleEarth™ time-series imagery, were used to identify training pixels. For forest cover loss, 339,589 pixels of forest cover loss training and 1,175,993 pixels of no forest cover loss training data were selected. For bare ground gain, 280,519 pixels of bare ground gain training and 12,308,780 pixels of no bare ground gain training were selected. To facilitate image interaction and assure a wide geographic spread of training sites, the WELD CONUS data were divided into 19 roughly square regions and training data delineated within each region for both forest cover loss and bare ground gain. Fig. 1 illustrates the approach using median growing season 2006 and 2010 imagery. The training method relies on the labeling of mixed pixels along class boundaries, forcing the interpreter to define more ambiguous pixels. In this way, the algorithm does not create a best-fit decision boundary between core

homogeneous spectral signatures, but is forced to work at the quantization level in discriminating class boundaries (Hansen, 2012). Hansen (2012) found that the targeting of spectral frontiers by training on class boundaries resulted in more accurate characterization of mixed pixels. In addition to training on inter-class boundaries, the variety of intra-class variation is targeted as well in training data derivation. The approach used in DeFries et al. (1998) through the presented study relies on expert image interpretation to build a training data set that captures all pertinent intra-class variation. For example, forest cover loss in CONUS includes logging, fire, stand mortality due to disease, and storm damage, all within a variety of forest types. Expert interpretation is used to build a training data set that captures national-scale forest loss and no loss sub-classes. The same procedure is used to derive training data for bare ground gain and no gain sub-classes.

2.3. Validation data

Our product assessment was based on GoogleEarth™ time-series imagery available within selected sample blocks. GoogleEarth™ time-series data consist of very high spatial resolution data from U.S. government agencies, such as the National Agricultural Imagery Program (NAIP) administered by the USDA Farm Services Agency, as well as direct commercial providers, such as GeoEye, Inc. The sub-5 m data enable the direct interpretation of tree crown presence and absence and bare ground presence and absence, when suitable data exist for the study interval of 2006 to 2010 (i.e. both early 2006 and late 2010 dates present).

2.4. Ancillary data

Results for gross forest cover loss were analyzed at the ecoregion scale using the ecoregional boundaries of Olson et al. (2001). An ecoregion is defined as a large area of land or water with similar biotic and abiotic characteristics (climate, topography, geology, soils, and natural vegetation). The combined environmental characteristics of an ecoregion represent its resource potential and probable responses to natural and anthropogenic disturbances. As such, they are a suitable

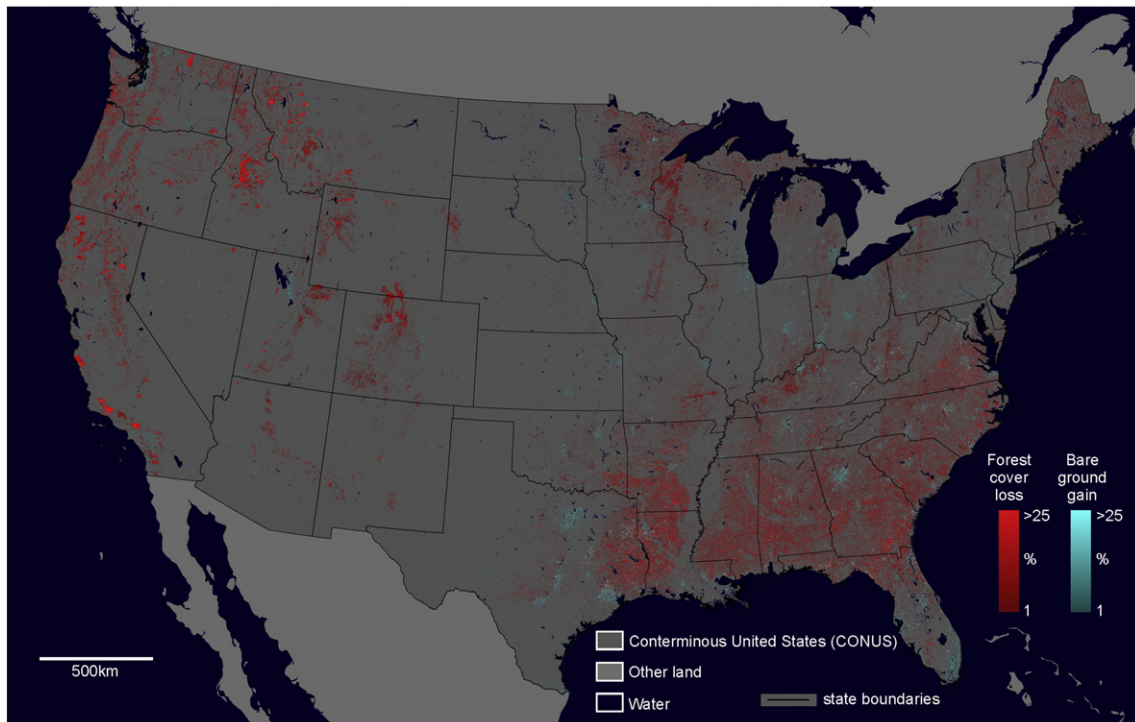


Fig. 4. Forest cover loss and bare ground gain from 2006 to 2010 for CONUS.

regionalization for the study of land cover extent and change (Loveland et al., 2002).

LiDAR (light detection and ranging) data from the GLAS (Geoscience Laser Altimetry System) instrument onboard the IceSat-1 satellite were used in an analysis of forest disturbance. GLAS was launched in January 2003 and collects laser pulses in an ellipsoidal footprint of approximately 65 m, spaced about 172 m apart along the orbital track. We downloaded the GLAS Release 28 (L1A Global Altimetry Data and the L2 Global Land Surface Altimetry Data) data set for the CONUS from the National Snow and Ice Data Center (NSIDC, <http://nsidc.org/data/icesat>). The GLAS data were screened using elevation, signal beginning, signal end and noise metrics derived from the GLAS waveforms; additional screening was conducted to remove the effects of cloud cover, slope and other deleterious factors. After this quality assessment phase, remaining viable GLAS shots were used to calculate canopy height (Goetz & Dubayah, 2011; Goetz, Sun, Baccini, & Beck, 2010).

Bare ground gain was studied in the context of urban development. To assess rates of change related to increasing urbanization, bare ground

gain was analyzed in the context of metropolitan statistical areas (MSAs) as defined by the U.S. Census Bureau (www.census.gov). Each MSA “consists of a core area containing a substantial population nucleus, together with adjacent communities having a high degree of economic and social integration with that core” and at least one U.S. Census Bureau-defined urbanized area of 50,000 or more population (<http://www.census.gov/population/metro/>). We used the subset of large Metropolitan Statistical Areas, or areas with 250,000 or greater 2010 population, to evaluate bare ground gain more probably related to urbanization than mining or other drivers of permanent or semi-permanent vegetation removal.

3. Methods

3.1. Product generation

The sequence of methods is illustrated in Fig. 2 for reference. The WELD-derived image metrics (Section 2.1) were the independent

Table 1
State forest totals for 2006 by varied per pixel canopy cover thresholds (Hansen et al., 2011), forest cover loss from 2006 to 2010, reported by percent forest cover loss by U.S. state.

State	>10% forest cover (km ²)	>30% forest cover (km ²)	>60% forest cover (km ²)	Forest cover loss (km ²)	%loss for > 10% forest cover
California	117,282	87,169	65,417	5082	4.33
Louisiana	68,944	63,184	55,103	2868	4.16
Georgia	106,651	100,225	87,631	4195	3.93
Alabama	99,440	93,665	83,960	3818	3.84
Idaho	78,261	68,884	57,957	2893	3.70
South Carolina	56,894	53,418	47,360	1883	3.31
Arkansas	83,371	77,160	70,561	2758	3.31
Mississippi	85,603	80,291	73,134	2787	3.26
Montana	82,006	69,665	56,907	2378	2.90
Washington	87,416	77,415	67,214	2449	2.80
Florida	78,592	69,456	54,744	2043	2.60
North Carolina	85,848	80,407	71,703	2183	2.54
Oregon	109,935	90,994	73,709	2686	2.44
Texas	120,743	91,309	68,340	2895	2.40
Wyoming	33,941	28,691	23,971	808	2.38
Virginia	74,588	70,000	63,702	1686	2.26
Utah	33,253	24,121	16,147	640	1.92
South Dakota	8976	5452	2868	150	1.67
Colorado	70,905	58,043	44,782	993	1.40
Oklahoma	47,502	36,546	29,421	661	1.39
Nevada	14,901	6083	2030	207	1.39
Tennessee	69,186	63,512	56,052	819	1.18
Minnesota	81,473	72,943	63,357	949	1.17
Delaware	2076	1813	1594	24	1.16
Maine	70,865	68,236	63,307	814	1.15
Wisconsin	76,854	70,989	63,379	653	0.85
Kentucky	61,522	55,791	48,998	518	0.84
District Of Columbia	57	39	29	0	0.84
Arizona	34,662	20,871	9207	253	0.73
Maryland	13,787	12,429	11,057	95	0.69
New Hampshire	20,899	20,311	19,181	140	0.67
Iowa	17,910	14,262	10,821	118	0.66
Michigan	93,130	85,858	75,382	568	0.61
Ohio	44,044	38,554	32,099	255	0.58
Indiana	28,057	24,764	20,846	161	0.57
Nebraska	8864	4955	2388	49	0.55
North Dakota	4337	2167	1053	23	0.52
West Virginia	52,823	50,119	46,117	272	0.51
Missouri	80,046	70,310	61,320	395	0.49
New Mexico	40,919	29,975	16,402	196	0.48
New Jersey	12,443	11,287	9945	50	0.40
Illinois	28,677	24,603	19,860	93	0.33
Massachusetts	16,487	15,581	14,068	51	0.31
Pennsylvania	80,891	74,342	66,161	240	0.30
Rhode Island	2114	1966	1787	5	0.23
New York	87,010	81,393	73,216	186	0.21
Kansas	16,730	10,776	7248	35	0.21
Connecticut	10,555	10,033	9277	21	0.20
Vermont	19,458	18,654	17,429	39	0.20
Alaska	na	na	na	na	na
Hawaii	na	na	na	na	na

variables and the change and no change labels from the training data (Section 2.2) the dependent variables. They were related to each other through a decision tree algorithm in order to extrapolate the estimation of forest cover loss and bare ground gain across the CONUS. Decision trees are well-established in remote sensing applications (e.g., Friedl and Brodley, 1997; DeFries et al., 1997; Hansen, Dubayah, & DeFries, 1996; Michaelson, Schimel, Friedl, Davis, & Dubayah, 1994) and have been used to generate the WELD Vegetation Continuous Field and Land Cover products (Hansen et al., 2011). Versions of tree model implementation include single trees, bagging, boosting and random forests (Ghimire, Rogan, Panday, Neeti, & Galiano, 2012). In this research, a bagged decision tree methodology based on the Classification and Decision Tree Methodology (CART) of Breiman, Friedman, Olshen, and Stone (1984) was used to classify the WELD bare ground gain and forest cover loss from 2006 to 2010. Decision trees are hierarchical classifiers that predict class membership by recursively partitioning a data set into more homogeneous subsets, referred to as nodes. The splitting procedure is followed until every pixel is discriminated from pixels of other classes, or until preset conditions are met for terminating the tree's growth. For classification trees, an entropy measure is used to split the data into nodes that are more homogeneous with respect to class membership than the parent node. The split that yields the maximum reduction in entropy is selected to build the classification tree model. In this research, a deviance measure reflecting node purity (Ripley, 1996) was used to terminate the tree model growth. A set of 25 trees was grown using a random 10% sampling of the training data sets with replacement for each tree (Breiman, 1996). Tree growth was terminated when additional splits decreased model deviance by less than 0.01% of the root node deviance. All per pixel results were ranked over the 25 trees, and the median probability of the bare ground gain and forest cover loss classes, respectively, was taken as the final result.

Annual estimates of each change dynamic were also generated from the epochal 2006–2010 interval. Individual date observations from the weekly mosaics were analyzed for pixels identified as having lost forest

cover or having gained bare ground. In this way, we are not using the time-sequential data to identify change as with other time-series approaches (Huang et al., 2009; Kennedy et al., 2010; Zhu, Woodcock, & Olofsson, 2013). Instead, we are looking for the date of disturbance given already flagged change pixels. For each change pixel, time-sequential normalized band 4/band 5 ratios, also referred to as the Normalized Difference Water Index (NDWI) (Gao, 1996), were used as inputs. NDWI has been used to map forest change using Landsat imagery (Wang, Lu, & Haithcoat, 2007) and employs longer wavelength bands less susceptible to atmospheric effects than NDVI, which incorporates the visible red band. Groupings of 4 consecutive observations were considered and the difference of the sums for the first two and last two dates calculated. For example, for acquisitions a_6 , a_7 , a_8 , and a_9 the difference value was calculated as $d = (a_6 + a_7) - (a_8 + a_9)$. The two-date sum was chosen to ameliorate the effects of noisy pixels not properly flagged in the quality assessment procedure. All difference values for the 2006–2010 weekly inputs were ranked. The maximum difference value was taken as the period when forest cover loss or bare ground gain occurred. The day of year of the third acquisition from the maximum difference calculation (the first known good acquisition after forest cover loss or bare ground gain) was recorded and stored in the WELD land cover change layers with the thousands place representing the year of the 2000 decade and the tens and ones places representing the week within the given year. For example, 8034 represents year 2008, week 34 for the date of land cover change. The date assessment was done exhaustively for all change flagged pixels. Fig. 3 is an example sequence of growing season imagery for bands 4 and 5 from a forest clearing disturbance in the Pacific Northwest. The method purposely avoids data poor times of year, typically winter and spring across the CONUS. This ensures the exclusive use of directly comparable growing season observations. However, change may occur in the off-season or in a season dominated by cloud cover, leaving some ambiguity as to which year the change actually took place. Fig. 3 illustrates such an example. The selection rule, as previously described, allocates the

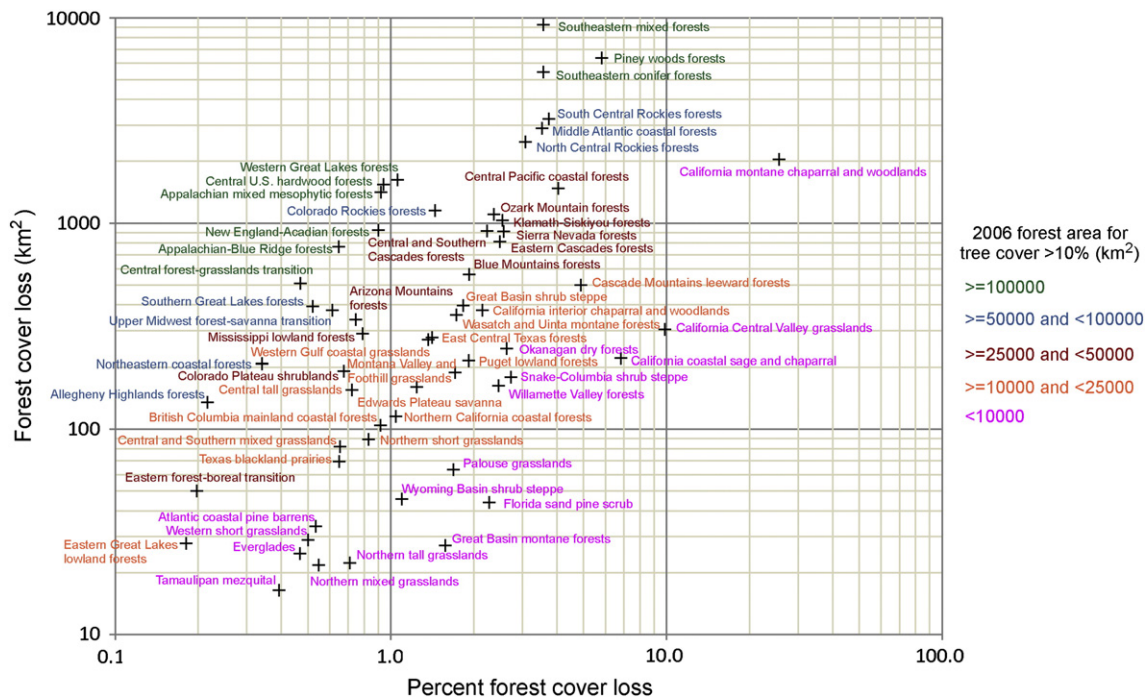


Fig. 5. Total gross forest cover loss and percent forest cover loss by ecoregion and total forest cover extent in 2006 where forest is defined as $\geq 10\%$ tree cover. The log–log plot was chosen in order to more clearly separate the ecoregions for visual display. Not included are the Flint Hills tall grasslands, Sierra Madre Occidental pine-oak forests, Nebraska Sand Hills mixed grasslands and Chihuahuan desert ecoregions, each of which have more than 1000 km² of forest cover and less 10 km² of forest cover loss. Also not included are the Mojave desert, Sierra Madre Oriental pine-oak forests, Canadian Aspen forests and parklands, South Florida rocklands, Sonoran desert, Sierra Juarez and San Pedro Martir pine-oak forests ecoregions, each of which have less than 1000 km² of forest cover.

change to the first known good acquisition after the change, in this case June 2008.

3.2. Analyses

Total and proportional gross forest cover loss was tabulated by state and ecoregion to capture spatial variation in the forest disturbance dynamic. Additionally, we employed a ‘core forest’ concept to quantify forested regions absent of change. A core forest was defined by thresholding the WELD VCF of percent tree cover at 60% in order to create an initial forest/non-forest layer. The 60% threshold focused the core forest analysis on dense tree cover and not on more open canopied woodlands and parklands. All forest cover loss pixels were buffered using a 1 km radius and VCF-thresholded forest pixels within this buffer removed. Remaining forest pixels were aggregated to a 300 m grid and all grid cells with $\geq 60\%$ forest retained. This aggregation step allowed for a minority of non-forest cover to exist within the core forests, such as water bodies and pastures. Contiguous blocks of these aggregated forest grid cells greater than or equal to 100 km² in extent were labeled as core forests.

GLAS LiDAR shots (Goetz & Dubayah, 2011; Goetz et al., 2010) were analyzed inside and outside of core forests under the assumption that regions exhibiting no forest disturbance will have different structural attributes compared to forests in proximity to disturbance. For bare ground,

we calculated the total area and proportion of area of bare ground cover gain by the 182 large Metropolitan Statistical Areas of the CONUS in order to differentiate trends in urbanization. Specifically, the census data from 2000 to 2010 were compared with bare ground gain total area from 2006 to 2010.

3.3. Validation

The forest cover loss and bare ground gain products were each assessed by separate validation studies. The sampling designs for each validation study were stratified one-stage cluster sampling designs. The cluster sampling unit was a 17 pixel by 17 pixel (510 m by 510 m) block of 30 m pixels. A 510 m by 510 m block could be hand-interpreted using GoogleEarth imagery while also representing a sufficient area for the sampling reference frame. The two populations of blocks defined for the validation were created using WELD percent tree cover and percent bare ground developed previously by Hansen et al. (2011), where a “population” here refers to the statistical population representing the area assessed by the validation sample. To define the bare ground gain population, the minimum percent bare ground of the 2006 annual layer and the 2006–2010 multi-year layer was used. The minimum percent bare ground reference layer was aggregated to the 510 m block scale and the population was defined as all blocks with at least 10% vegetation. To define the population for the forest

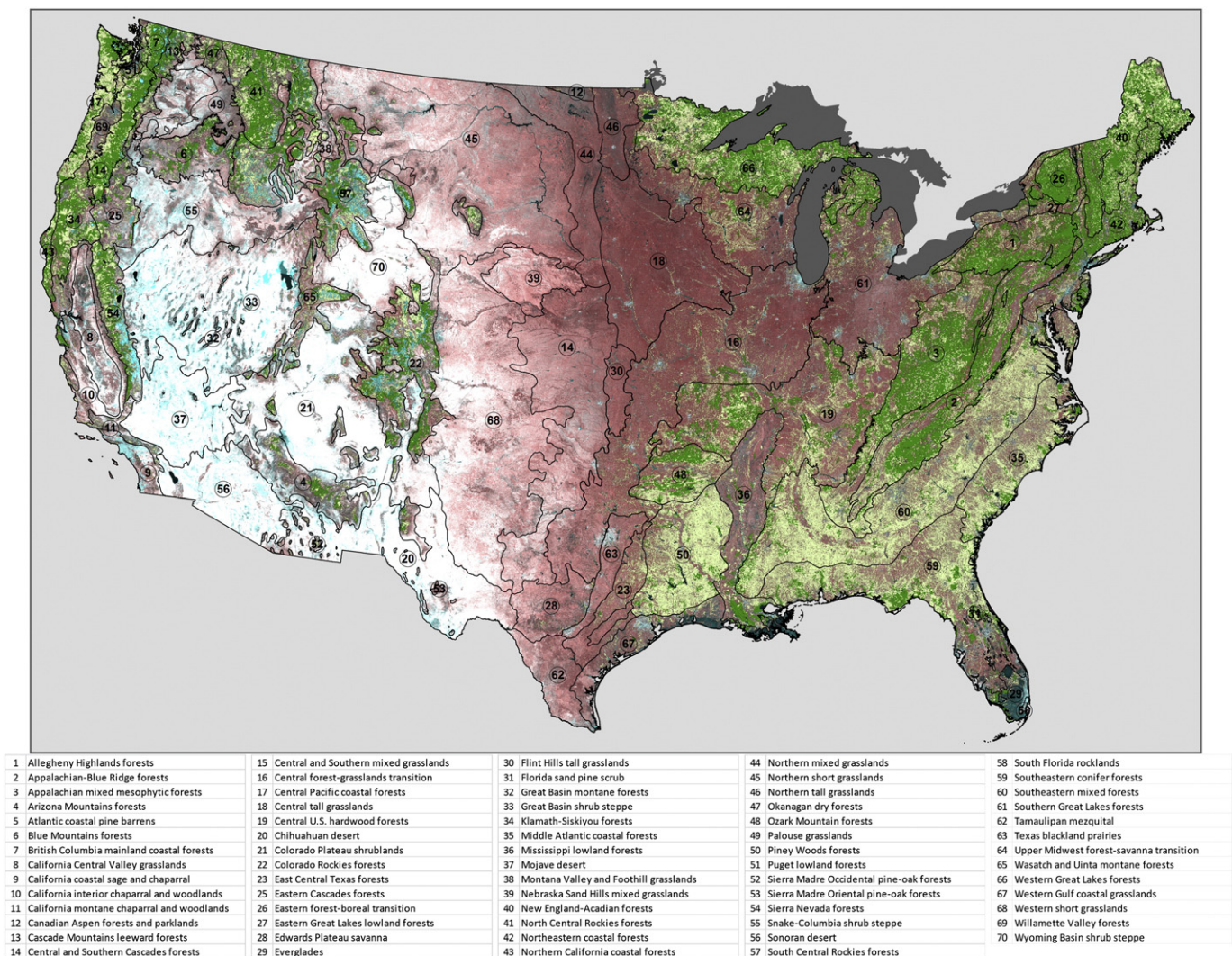


Fig. 6. Map of forest cover where dark green is core forest and beige other forest cover. Ecoregions are from the World Wildlife Fund (Olson et al., 2001). The background image is a 5-year growing season median observation for ETM+ bands 4, 5 and 7 in r-g-b.

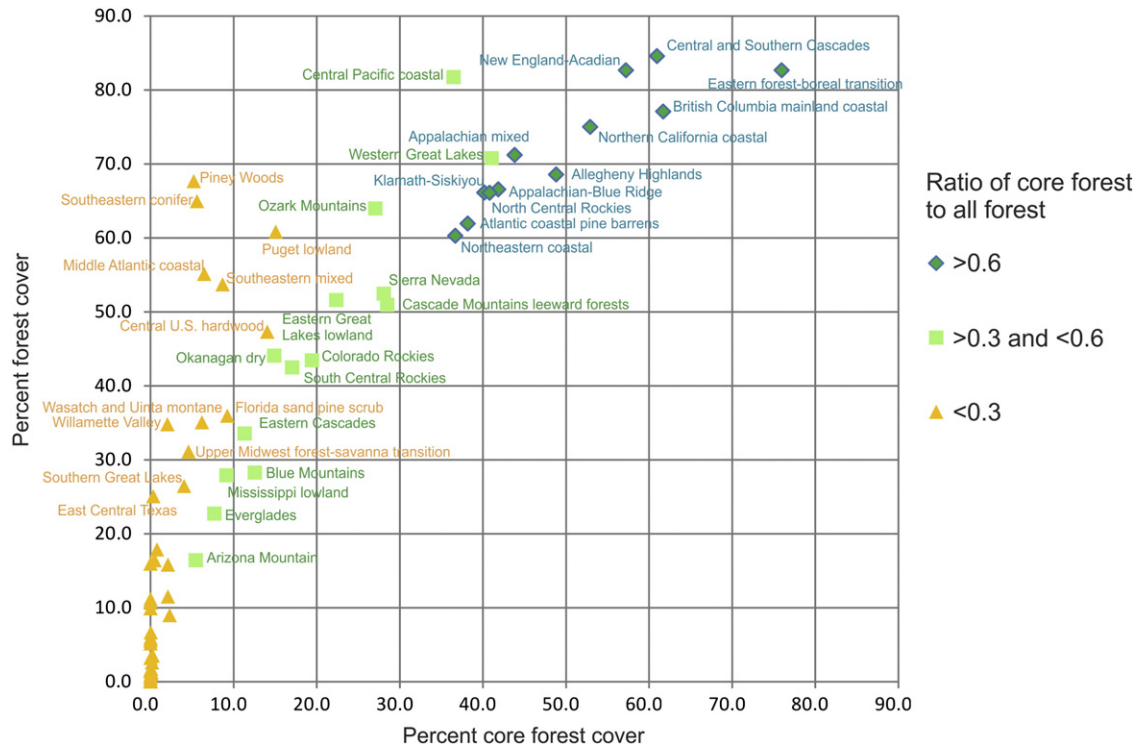


Fig. 7. Area of total forest cover versus core forest cover by ecoregion.

cover loss validation, the maximum tree cover extent was calculated using the 2006 annual percent tree cover layer and the 2006–2010 multi-year layer. This product was also averaged to the 510 m block scale and the population was defined as all blocks with at least 10% tree cover. The populations of 510 m blocks (clusters) were then partitioned into two change strata, one with $\leq 1\%$ change and one with $> 1\%$ change. For forest cover loss, the $\leq 1\%$ stratum totaled 11,608,710 blocks and the $> 1\%$ stratum 1,609,138 blocks. For the bare ground gain population, the $\leq 1\%$ change stratum consisted of 28,872,096 blocks, and the $> 1\%$ stratum had 483,981 blocks. For each stratum in each population (forest cover loss and bare ground gain), a simple random sample of 75 blocks was selected.

The sample blocks were then displayed in GoogleEarth™ and, for blocks with suitable imagery, change digitized. On-screen delineation of forest cover loss and bare ground gain were performed for the respective sample block populations. If GoogleEarth™ imagery was not suitable, the sample block was discarded and the next block on a randomized list replaced the discarded block (for the forest loss sample, 10 blocks were replaced as unusable, and for the bare ground gain sample, 33 blocks were replaced). Change consisted of tree crown loss and bare ground gain. National estimates of overall, user's, and producer's accuracies were produced from the stratified one-stage cluster sample for each change product, where the estimates apply to the 30 m pixels.

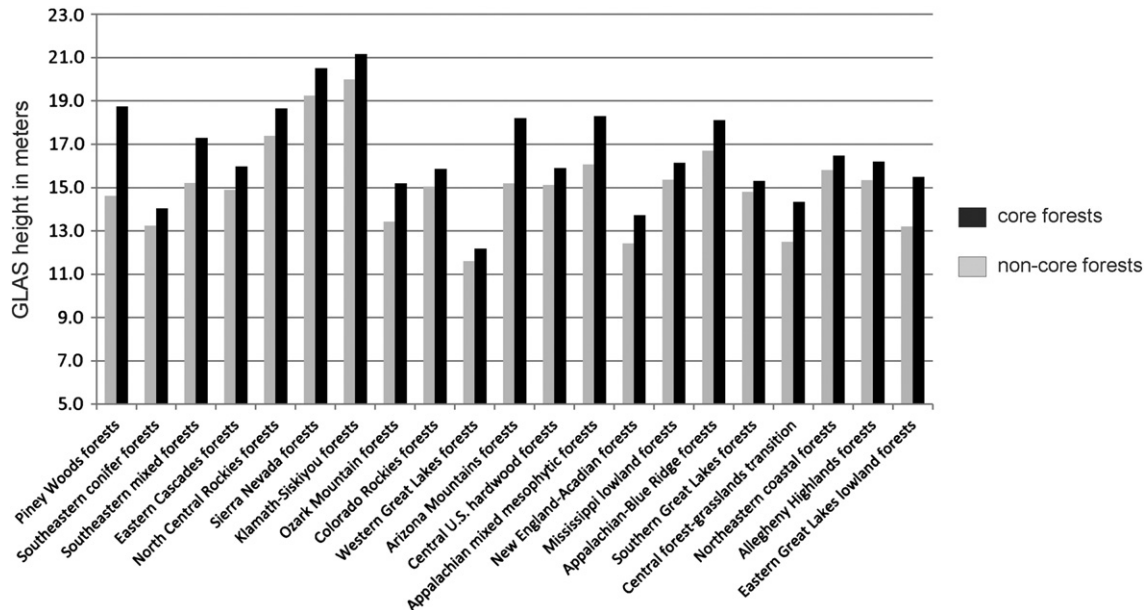


Fig. 8. Mean GLAS height for forest pixels inside and outside of core forest areas for ecoregions with 500 or more shots for both forest types.

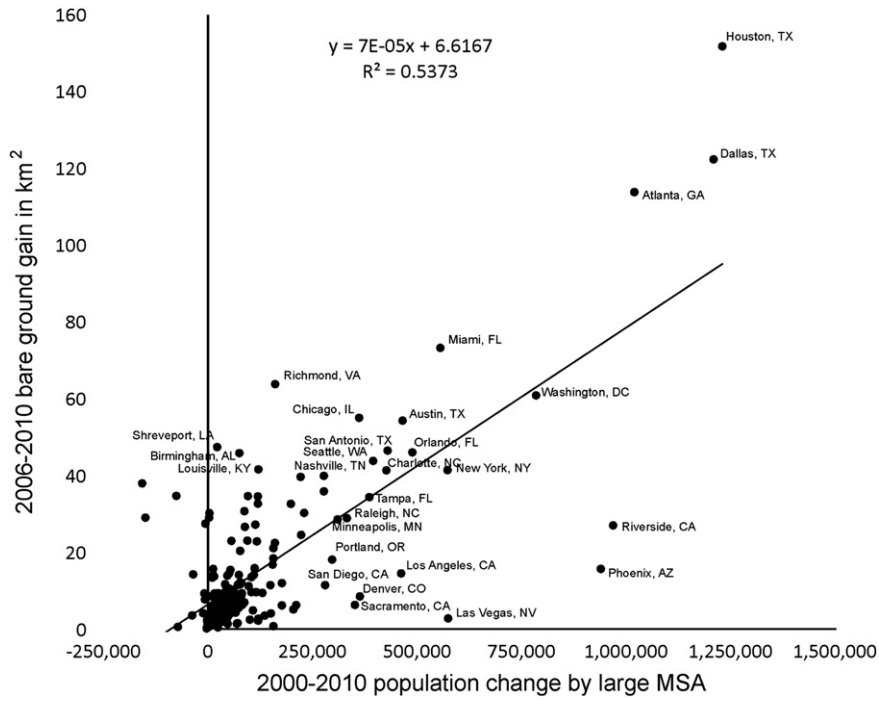


Fig. 9. Bare ground gain, 2006–2010 versus population change, 2000–2010 for large metropolitan statistical areas of CONUS.

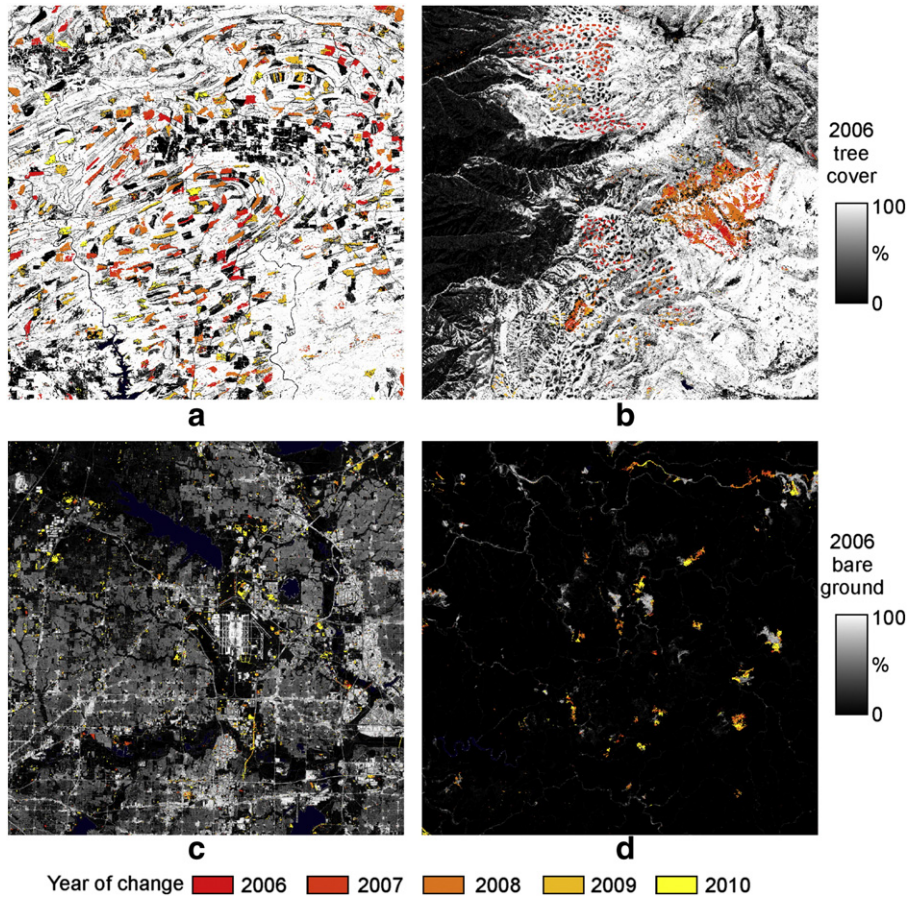


Fig. 10. Annual change for subsets 40 km by 40 km in size for a) forest cover loss in the Ouachita Mountains of southeast Oklahoma centered at 34 20N, 95 00W, b) forest cover loss in the northern Sierra Nevada centered at 40 11N, 121 36W, c) bare ground gain for the metropolitan area of Dallas/Fort Worth, Texas centered at 32 53N, 96 69W, and d) bare ground gain in rural Kentucky and West Virginia centered at 37 30N, 82 30W. Percent tree cover (a and b) and percent bare ground (c and d) are shown in gray-scale.

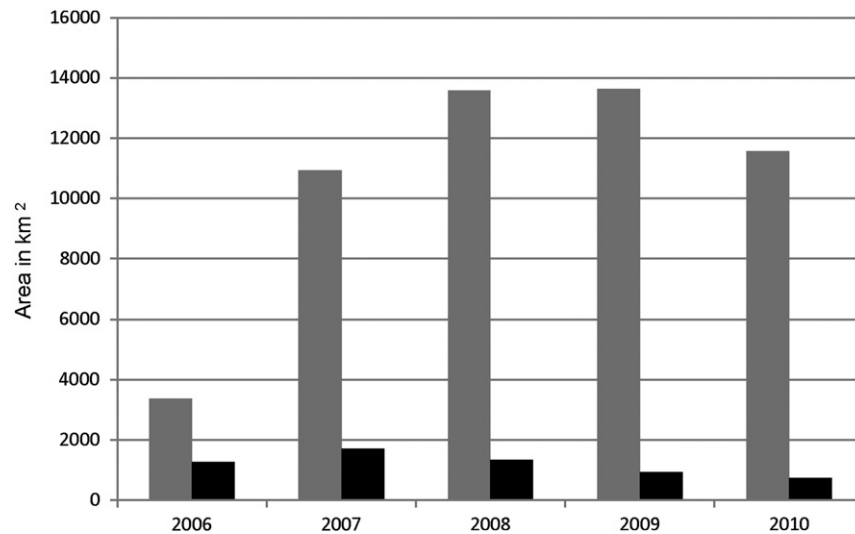


Fig. 11. CONUS estimated area of annual forest cover loss (gray) and bare ground gain (black).

4. Results

The gross forest cover loss and bare ground gain products for CONUS are shown in Fig. 4. The data are shown as percent change per the aggregated 510 m grid which was used to create the validation sampling frame. The same enhancement is used to visualize the overall patterns of the two dynamics and the dramatic difference in overall forest cover loss compared to bare ground gain. For this figure, any 510 m cell that has 1% change or greater is shown in red or cyan color scale. Overestimations of forest cover loss due to data poor Landsat paths and scan gaps are visible in this enhancement.

4.1. Gross forest cover loss

Mapped gross forest cover loss for CONUS from 2006 to 2010 totaled 53,084 km². State totals for 2006 forest cover and 2006–2010 forest cover loss are shown in Table 1. In the 4-year interval, 2.3% of CONUS forest cover was disturbed according to the WELD result, when applying a 10% tree cover threshold to define reference forest cover area. Results by ecoregion are shown in Fig. 5. Southeastern ecoregions have the highest total gross forest cover loss and California chaparral ecoregions the highest proportional forest cover loss. Fig. 6 depicts the geographic extent of the core forests and Fig. 7 is a plot of percent total forest area versus percent core forest area by ecoregion. Ecoregions in blue have 60% or greater total forest area as core forests. These ecoregions consist of large blocks of forest cover absent of stand-replacement disturbance and include areas of the Pacific Northwest and Atlantic northeast. An intermediate category is shown in green where core forests account for 30–60% of total forest area and includes a geographically diverse set of ecoregions. The yellow class represents ecoregions where core forests account for <30% of total forest area. Ecoregions in this category with relatively high total forest area are found mainly in the Southeastern United States. Fig. 8 shows a comparison of ecoregions with at least

Table 2

Forest cover loss (error matrix entries are % of area).

Google Earth				
Map	No Loss	Loss	Total	User's acc (SE)
No loss	97.63	0.64	98.27	99.4 (0.2)
Loss	0.38	1.35	1.73 (0.6)	78.2 (3.2)
Total	98.01	1.99 (0.6)	Overall 98.3 (0.6)	
Prod acc (SE)	99.6 (0.1)	68.0 (4.7)		

500 GLAS shots for both core and non-core forests and a 95% *t*-test confidence interval. For all of the ecoregions in Fig. 8, the mean GLAS height for the core forests lacking disturbance is consistently greater than the mean GLAS height within the non-core forests.

4.2. Bare ground gain

Mapped gross bare ground gain for CONUS from 2006 to 2010 totaled 5974 km². Nearly one-half of the total bare ground gain (47%) occurs within large Metropolitan Statistical Areas (MSAs). These MSAs themselves cover 55% of the CONUS land area, meaning proportionally more bare ground gain is found outside of MSAs. A comparison of bare ground gain to MSA population growth was made using 2000 to 2010 census data and is shown in Fig. 9. The overall *r*² of 0.53 clearly indicates the limitation of the bare ground gain product in capturing land use conversions associated with urban development, particularly when the development occurs in low vegetation areas (see Discussion section).

4.3. Annual change

Fig. 10 shows the gross forest cover loss allocated annually for a portion of a) southeast Oklahoma in the western Ouachita Mountains and b) northern California in the Sierra Nevada Mountains along with gross bare ground gain allocated annually for c) the city of Houston, Texas and d) the Kentucky/West Virginia border. The CONUS annual totals for both dynamics are shown in Fig. 11.

4.4. Validation

Validation results are shown in Tables 2 and 3 for forest cover loss and bare ground gain, respectively. Seventy-five blocks in each of the change and no change strata were analyzed; their distributions across CONUS are shown in Fig. 12. Fig. 13 shows the area totals for forest

Table 3

Bare ground gain (error matrix entries are % of area).

Google Earth				
Map	No gain	Gain	Total	User's acc (SE)
No gain	99.887	0.034	99.921	99.9 (0.01)
Gain	0.045	0.033	0.078 (0.016)	42.3 (10.0)
Total	99.932	0.067 (0.020)	Overall 99.92 (0.02)	
Prod acc (SE)	99.95 (0.01)	49.3 (9.3)		

cover loss and bare ground gain, respectively, for 1) the validation sample blocks using GoogleEarth™ very high spatial resolution imagery, 2) the same sample blocks using the WELD land cover change product, and 3) the total area of change from the full WELD land cover change product.

The per pixel output of the decision tree algorithm used in this study is a probability of class membership, in this case the membership of being in the change category under consideration. By varying the probability threshold, different realizations of the product can be created. Broich et al. (2011) used a sliding threshold to match producer's and user's accuracies when comparing a wall-to-wall map probability

layer with a set of validation sample blocks. This approach ensured that the total area portrayed in the map matched that of the validation data set. For this study, we did not employ this approach, but do present three realizations for comparison with the validation data. Fig. 14 illustrates the relationship between the validation data and 25%, 50% and 75% thresholded change products. For mean simple and absolute differences, the 50% threshold produced the smallest residuals for both forest cover loss and bare ground gain validation blocks. Pixels with a probability of change class membership of 50% or greater were labeled as change in the final product. Five blocks are highlighted in Figs. 12 and 14 and displayed in Figs. 15 and 16. These samples represent the

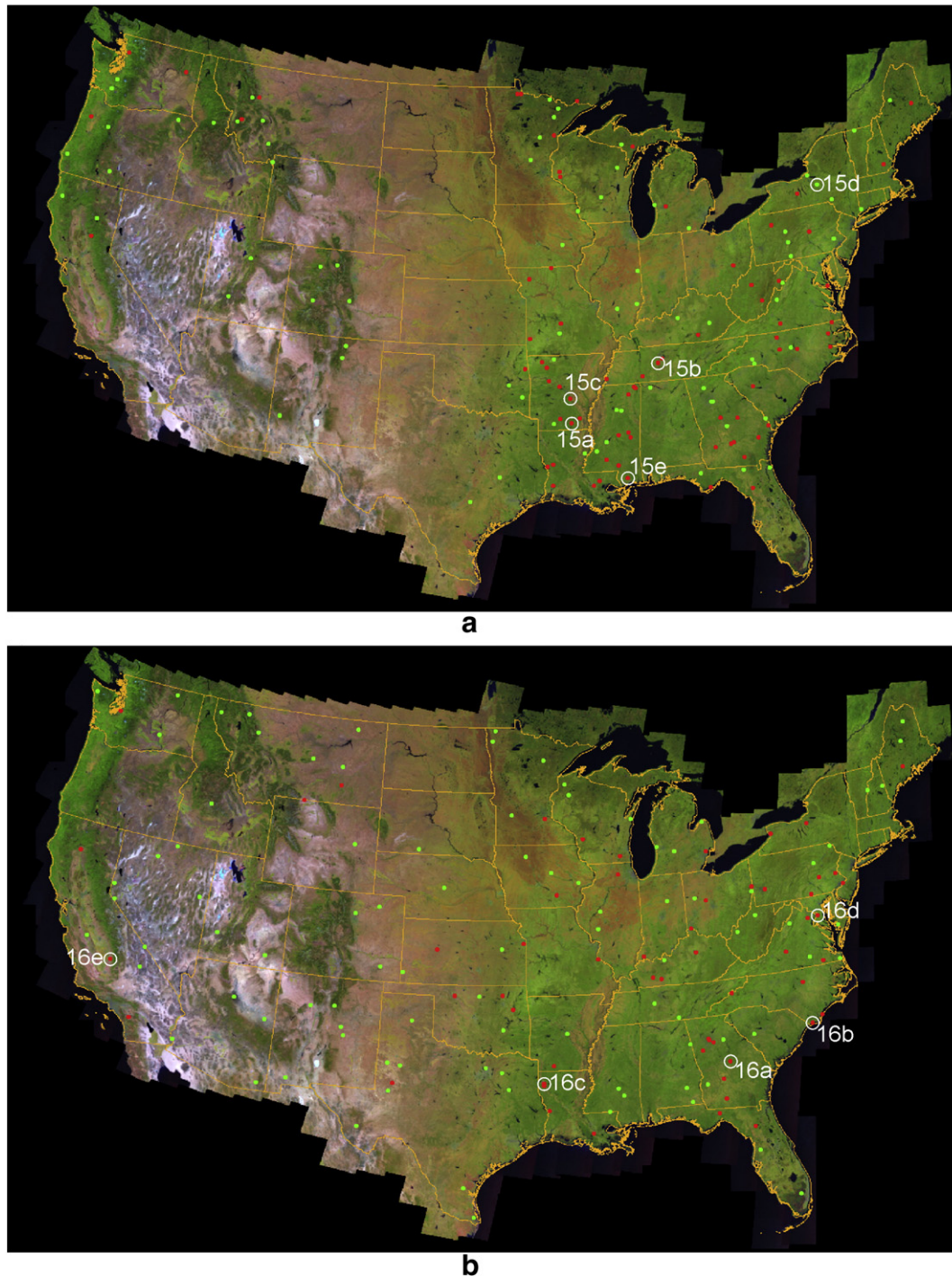


Fig. 12. Validation sample blocks for a) no forest cover loss (green) and forest cover loss (red) strata, and b) no bare ground gain (green) and bare ground gain (red) strata. Background image is 5–4–3 of 5-year growing season median imagery. Highlighted blocks are referred to in the text and are shown in Figs. 15 and 16.

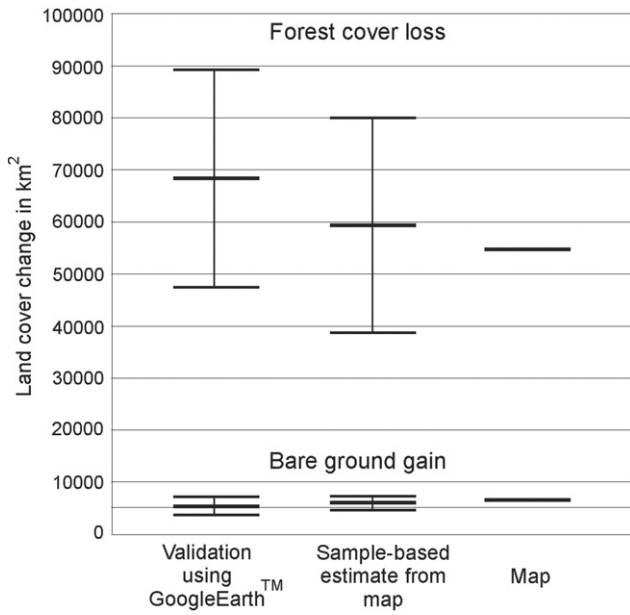


Fig. 13. Estimation of a) forest cover loss and b) bare ground gain for the validation sample blocks using GoogleEarth™ very high spatial resolution imagery, the same sample blocks using the WELD land cover change product, and the total area of change from the full WELD land cover change product. Bars for sample-based estimates represent \pm one standard error.

following five cases: high change agreement, medium change agreement, low change agreement, highest change commission error and highest change omission error. These examples will be referred to throughout the validation results and discussion sections.

The results for the per pixel (30 m) accuracy assessment of the population of forest cover loss validation blocks are shown in Table 2. Based on the sample, the map estimates 1.73% forest cover loss, and the GoogleEarth™ validation estimates 1.99%, for an estimation area of omission of 0.26%. For every four correctly labeled forest cover loss pixels, there is roughly one forest loss pixel mapped in error (user's accuracy of $1.35/1.73 = 0.78$). For every two correctly labeled forest

cover loss pixels, there is nearly one forest cover loss pixel omitted (producer's accuracy of $1.35/1.99 = 0.68$).

The results of the per pixel accuracy assessment of the population of bare ground gain validation blocks are shown in Table 3. Based on the sample, the map estimates 0.078% bare ground gain, and the GoogleEarth™ validation estimates 0.067%, for an area of commission of 0.011%. For every two correctly labeled bare ground gain pixels, there are nearly three bare ground gain pixels mapped in error (user's accuracy of $0.33/0.78 = 0.42$). For every correctly labeled bare ground gain pixel, there is roughly one bare ground gain pixel omitted (producer's accuracy of $0.33/0.67 = 0.49$).

A second validation intercomparison was made to differentiate errors more likely to be associated with geolocation and possible effects related to scale than with 'blunders' or errors located in isolation from correctly mapped change. In this assessment, any omission or commission errors adjacent to each other or to agreed change were not counted as error. Only omission or commission errors that occurred in isolation (not along a shared border or diagonal to each other) were counted as error in this reanalysis. For example, Fig. 15c has 7 change pixels in agreement, 6 pixels of mapped change and 6 pixels of validation change. The user's and producer's accuracies for this block are both 46% (6/13). However, the map product clearly depicts the local forest change dynamic, and under the revised definition of agreement, all errors in Fig. 15c were relabeled as agreement.

For forest cover loss, the user's accuracy is 93% and the producer's accuracy 89% under this assumption. Restating accuracy in simpler terms, for every 8 correctly mapped forest cover loss pixels, there is roughly one mapped in error adjacent to correctly mapped change and one mapped in error located more than one pixel from correctly mapped change. For every 7 correctly mapped change pixels, there are roughly two change pixels omitted that are located adjacent to correctly mapped change and one change pixel omitted located more than one pixel away from true change.

Under this same assumption, the bare ground gain user's accuracy is 62% and the producer's accuracy 75%. Restating accuracy again in simpler terms, for every 4 correctly mapped bare ground gain pixels, there are roughly two mapped in error adjacent to correctly mapped change and another four mapped in error located more than one pixel from correctly mapped change. For every 5 correctly mapped change pixels, there are roughly 2.5 change pixels omitted that are located

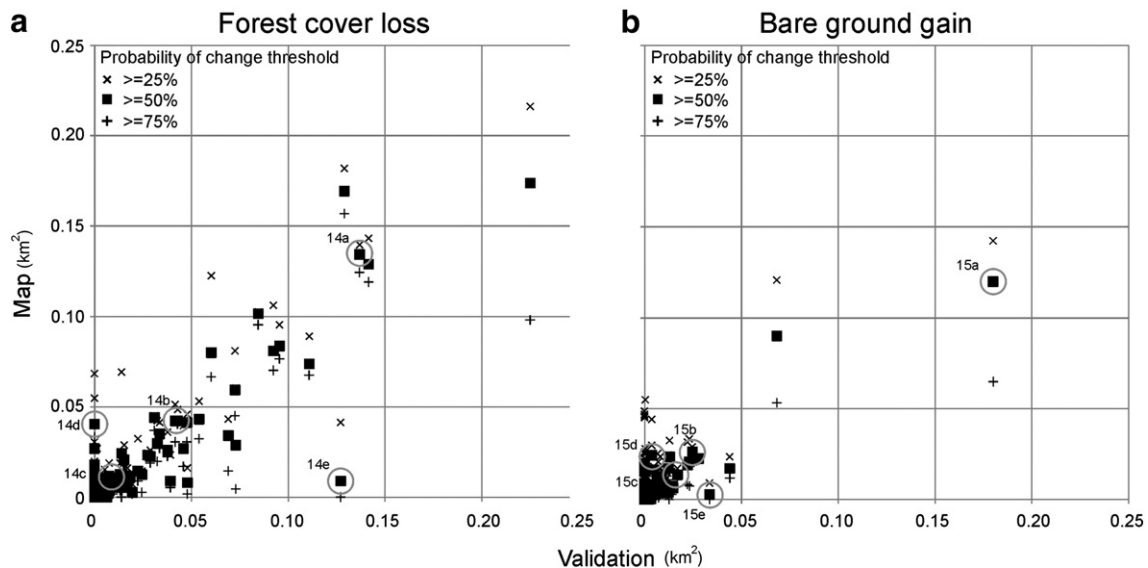


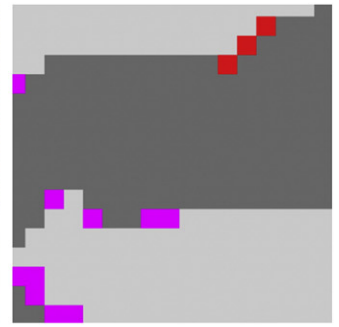
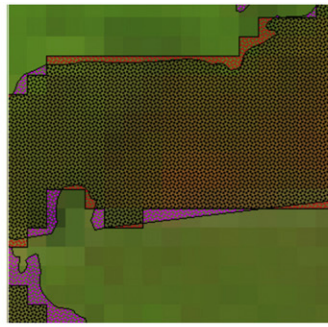
Fig. 14. Plots of per block reference versus map data where reference validation data are derived from GoogleEarth™ very high spatial resolution imagery and map data are derived using a sliding probability threshold of class membership. The final maps of change for both forest cover loss and bare ground gain were made for pixels with a 50% or higher probability of change class membership. Circles refer to blocks illustrated in Figs. 15 and 16.



a 9/18/2006



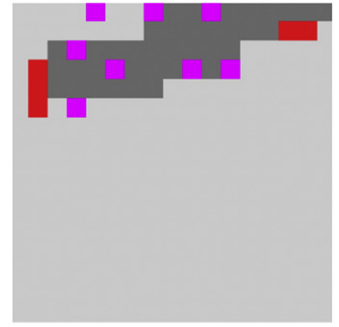
10/14/2010



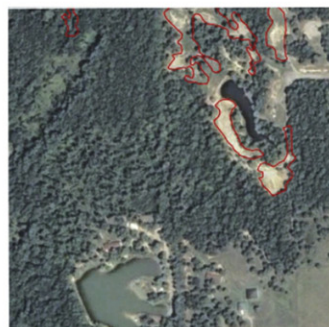
b 3/31/2006



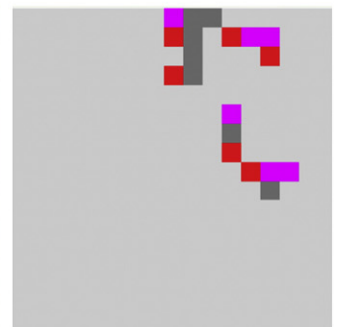
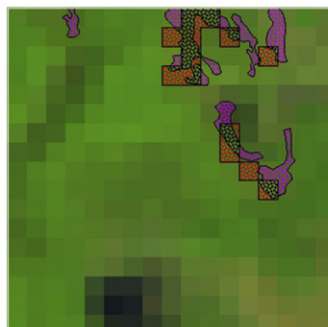
8/23/2010



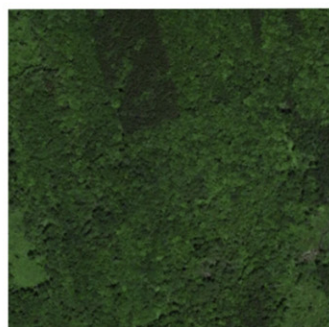
c 9/18/2006



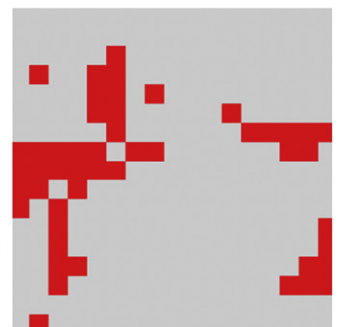
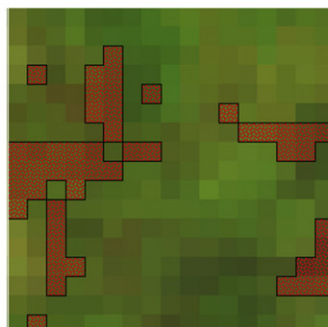
10/14/2010



d 11/25/2006



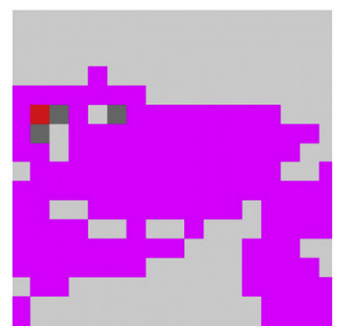
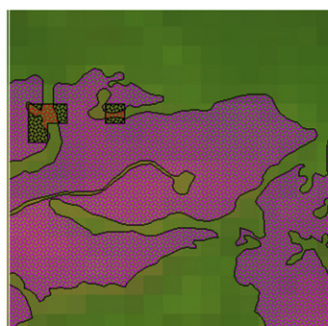
6/3/2010



e 5/31/2006



9/30/2010



adjacent to correctly mapped change and 2.5 change pixels omitted located more than one pixel away from true change.

5. Discussion

Regional subsets of the CONUS forest cover loss and bare ground gain product for 2006–2010 are displayed in Fig. 17. Fig. 17a of the Pacific Northwest shows a widespread forest cover loss dynamic, consisting principally of fire and logging. Bare ground gain is concentrated in the states of Washington along the Puget Sound and Oregon within the Willamette Valley. Fig. 17b highlights the most rapid urbanization dynamic detected, that of Texas. Newly established mining and pads for oil and gas drilling are also widespread in this region. The subset of Fig. 17c illustrates bare ground gain along the major highways linking the urban corridor from Washington, D.C. to Charlotte, North Carolina, as well as a more general forest cover loss dynamic throughout the Atlantic Coastal Plain and Piedmont regions. Surface mining, including mountain top removal mining along the West Virginia and Kentucky border, appears white as it results in both forest cover loss and bare ground gain. A strip of commission error is also seen in the middle of West Virginia due to SLC-off data gaps and the resultant lack of viable observations. Landsat 5 data added to the WELD inputs would ameliorate this data limitation. As part of the WELD land cover product suite, a layer consisting of the number of good (not cloudy) acquisitions per WELD grid cell over the 5 annual growing seasons is provided at the WELD project website. This layer can be used as an indicator of product quality. No post-processing was performed on the presented products to correct errors related to data limitations.

5.1. Forest cover loss

Regional variation in the forest cover loss product is high. Observed loss in California is largely related to fires in the past decade (Syphard et al., 2008). Southeastern forest cover loss is largely the result of intensive plantation forestry, where forests function more as a commodity crop. Drummond and Loveland (2010) highlight this change dynamic as the primary source of gross land cover change in the Eastern United States. The Rocky Mountain ecoregions are the site of intensive forest mortality due to mountain pine beetle outbreaks (Collins et al., 2010). Ecoregions of the Mid-Atlantic and New England have considerable forest cover and relatively low forest loss.

The southeastern U.S. has proportionately the least area of core forest compared to total forest area. While this region of the U.S. has extensive forest cover, little is identified as core forest, except for limited areas of national forest and bottomland hardwood forest. This result reflects the region's intensive forestry land use. The northeast U.S. has several extensive core forest zones with the Adirondack mountains of the Eastern forest-boreal transition ecoregion having the highest proportion of core forest to total forest area of all U.S. ecoregions. Several Pacific Northwest ecoregions have high proportions of core forest area, as do the northern Rocky Mountains. Of the four ecoregions with greater than 30% core forest and greater than 2% forest cover loss (Central and Southern Cascades forests, Klamath–Siskiyou forests, Central Pacific coastal forests and North Central Rockies forests), three are in the Pacific Northwest. Having both significant core forest and high rates of change indicates that forest disturbance is more clustered in these ecoregions. It must be noted that the period of study is short, and areas having experienced logging in the recent past, but not within the 2006 to 2010 interval, will be classified as core forests. Extension of the method to decadal or longer intervals would certainly reduce the extent of classified core forest.

Forests outside of core forests exist in proximity to forests experiencing change and are assumed to be part of an ongoing dynamic of forest land use. This assumption does not generically hold for other proximate causes of forest cover loss such as fire, disease and storm damage. Regardless, core forests are posited to be structurally different than other forests as they are more likely to represent natural and longer-lived stands of tree cover. This is not a given for all areas, as intensive plantation forestry could often lead to forest stands of greater structural height than natural stands. Regardless of these caveats, twenty-one ecoregions were found to have significantly different GLAS-derived mean canopy heights when comparing core and non-core forests.

These results support the use of sampled LiDAR data to assign structural attributes to thematic forest classes derived using spatial contextual information (Hudak, Lefsky, Cohen, & Berterretche, 2002). Results reflect those of Margono et al. (2012) who showed that primary intact forests of Sumatra, Indonesia exhibited higher GLAS-derived mean height and height of median energy values than primary degraded and other non-primary forests. Margono et al. (2012) employed the Intact Forest Landscape concept (Potapov et al., 2008) to delineate primary intact forests. The core forest analysis could provide an additional basis for differentiating generic forest cover in assessing the provision of ecosystem services.

5.2. Bare ground gain

Observable drivers of bare ground gain are primarily residential, commercial and infrastructure development within MSAs. Outside of MSAs, a more complicated conversion process is seen that includes the dynamics observed inside MSAs as well as mining, expanding infrastructure related to energy extraction and agriculture, and natural change dynamics such as meandering rivers. For the fastest growing cities, a corresponding expansion of bare ground land cover is seen. However, the local environmental context appears to either enhance or diminish the capability of the bare ground gain layer to quantify urban land conversions. For cities with high vegetative cover, including Houston, Dallas, Atlanta, Washington and Miami, a strong correlation is observed. However, for cities in desert or semi-desert environments with comparable population growth, including Riverside, Phoenix, and Las Vegas, there is no commensurate increase in bare ground.

The impervious surface products prototyped by Goetz et al. (2003) employed in change detection by Sexton et al. (2013a) are a subset of the change detected here as bare ground gain. By focusing on MSAs, there is a more direct comparison thematically, as most bare ground gain is linked to development and increased impervious surface. Variation in rates of urbanization in the form of impervious surface relates to a host of local drivers including formal land use planning, economic and demographic growth, and other factors. The method presented here is meant to be more easily implemented at regional to global scales while still capturing land cover conversion in quantifying urban expansion. The fact that the majority of bare ground gain was mapped as having occurred outside of the large MSAs points to the need for more synoptic quantification of this dynamic.

5.3. Annual change

A potential bias of the method is seen in the annual change allocations, as relatively less change is detected in the first and last years of study. This is likely due to the training data collection which employed median growing season imagery and reveals a limitation of metrics in detecting change. While anniversary date methods could better control for start-end change estimation, data quality and availability issues limit

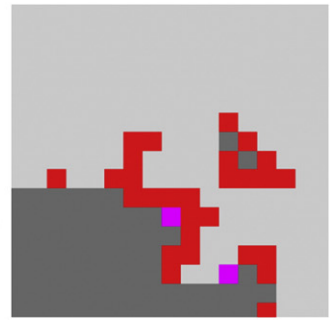
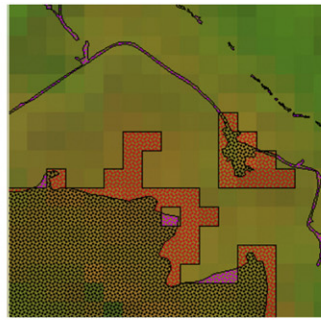
Fig. 15. Example validation blocks for forest cover loss. Left to right are 1) reference GoogleEarth™ validation time 1 imagery, 2) time 2 imagery, 3) forest cover loss over Landsat reference image where gray is forest cover loss agreement, red is WELD forest cover loss and magenta is validation forest cover loss, and 4) visual confusion matrix where dark gray equals forest cover loss agreement, light gray no forest cover loss agreement, red commission error and magenta omission error.



a 9/27/2006



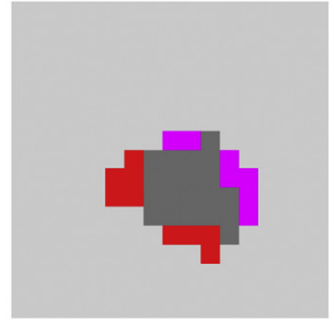
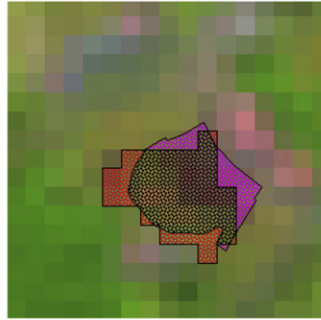
10/7/2010



b 10/17/2005



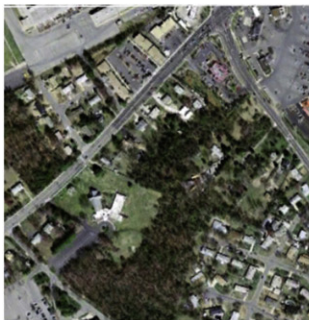
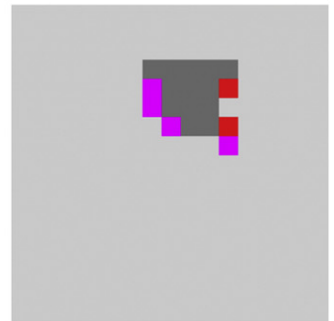
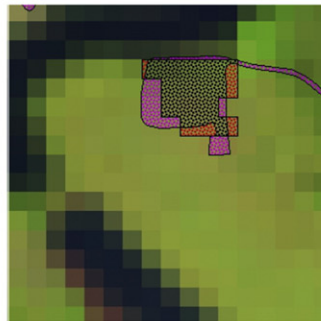
10/23/2010



c 10/2006



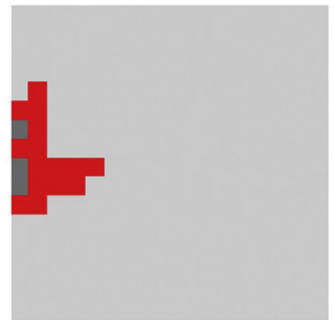
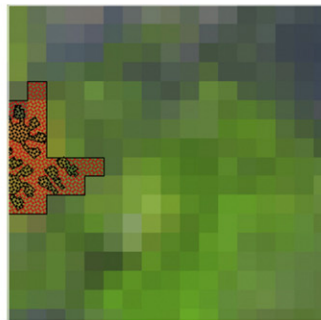
11/2010



d 3/2006



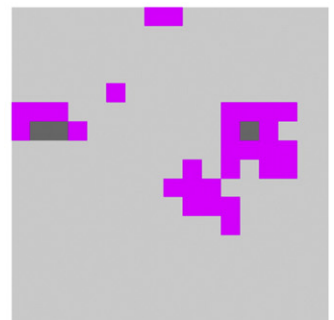
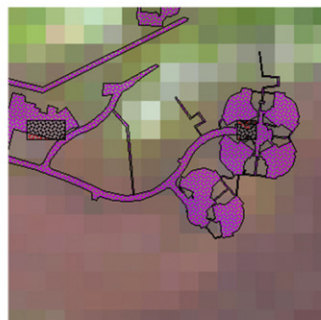
8/2010



e 8/5/2006



9/16/2010



such approaches. Potapov et al. (2012b) used 'end-point' metrics tied to anniversary start-end dates to derive training data. Such an approach, as well as incorporating non-growing season imagery, could improve annual detection and allocation for beginning and end years when using time-integrated spectral metrics. Additionally, a host of time-series applications based on Landsat data are improving timing-specific detection of change (Huang et al., 2009; Kennedy et al., 2010; Zhu et al., 2013), though all will have challenges in allocating change at the beginning and end of the time-series.

5.4. Validation

Wickham et al. (2013) performed a validation of the USGS National Land Cover Database (NLCD) change product from 2001 to 2006 (Xian et al., 2009). While the time interval for the NLCD change layer was different than this study, the interval length was similar and covered the same area, CONUS. Wickham et al. (2013) estimated national-scale producer's accuracy for forest loss at 82% and user's accuracy at 30%, compared to this study which yielded 78% and 68%, respectively, for the same measures. The closest change theme to the WELD bare ground gain layer is the NLCD urban gain class. Wickham et al. (2013) estimated national-scale producer's accuracy for urban gain at 72% and user's accuracy at 18%, compared to this study which yielded 42% and 49%, respectively, for the same measures. The presented study has more balanced producer's and user's accuracies and less omission error for both change classes. However, commission error is higher in the WELD bare ground gain class than in the NLCD urban gain class.

Fig. 15 provides examples of the forest cover loss validation sample blocks. Forest agreement cases are self-explanatory (Fig. 15a, b and c) and represent high, medium and low forest cover loss agreement. A considerable proportion of disagreement is due to apparent misregistration between the two data sets and differences in observational scale. The highest commission error of Fig. 15d is a result of the paucity of observations and the resulting false change detected in ETM + Scan Line Corrector-off gaps. This sample block had the lowest mean observation count (average number of valid weekly observations for all pixels in the block during the study period, in this case 22 compared to a mean of 40 for all blocks), reflecting an uneven richness in data not only due to SLC-off gaps, but also cloud cover (Ju & Roy, 2008). For cloud-affected areas, especially in deciduous forests such as this region of New York State, false change mapping is more likely. The highest omission error of Fig. 15e is not as easily explained, as the block has a slightly above average mean observation count of 43. Of all samples, this is the largest outlier, with a difference of reference minus map forest cover loss area of 0.106 km². The second largest residual is less than one-half this value. The sequence of GoogleEarth™ images depicts an already thinned stand in 2006 that is cleared in a series of steps, possibly obscuring the disturbance from detection in the applied set of decision trees. Outliers such as Figs. 15d and 15e deleteriously affect the overall accuracy of the product.

Fig. 16 provides examples of the bare ground gain validation sample blocks. Agreement cases are self-explanatory (Fig. 16a, b and c) and include per pixel errors related to misregistration and scale. For commission error, the example shown in Fig. 16d illustrates a definitional challenge when mapping bare ground change. The development of a suburban bedroom tract community often includes a temporary, but dramatic, denudation of the landscape. Only the housing units and roads persist as permanent conversion. However, the bare ground gain map product captured the entire disturbed area as bare ground gain. This type of error is common and points to a temporal limitation

in both identifying and assigning a pixel to the bare ground gain class. Issues concerning how long a bare ground signal should persist before it can reliably be labeled as permanent or semi-permanent land cover change will require more years of data to adequately address. Omission error is shown in Fig. 16e and illustrates a signal limitation for a drier summer climate in the Central Valley of California. Improving the feature space to include winter growing season data for the Mediterranean climate of coastal California would allow for detection of this change. Regardless, the lack of sensitivity of the bare ground change model to land conversion in low vegetation ecoregions is a limitation that needs to be improved upon in future product iterations.

The ability to quantify areal change using a continental-scale algorithm is a challenge. As larger areas are analyzed, a more general model fit is required. A large area analysis is forced to combine various change dynamics into a single rule set, a generalization that may limit map accuracy; alternatively, a stratified approach may better fit local change dynamics, but potentially sacrifice large area consistency. Moving forward, this tension between global approaches and stratified ones meant to better fit local conditions will need to be resolved. The validation data are a good example of this issue. By deriving individual interpretations per block, i.e. fitting to local conditions, the validation data are accepted as being of higher quality than the map which applies a single interpretation, or model, to the entire study area. It is worth noting that a national or global land cover product using a single rule set can be validated using strata based on ecological (biomes for example) or administrative sub-units (large countries for example). Such a validation exercise could be used to formally quantify error in justifying a move to a stratified mapping approach. Despite these concerns, the validation of the WELD-derived CONUS-scale model compare favorably to the per scene NLCD validation study of Wickham et al. (2013).

6. Conclusion

Products generated for this study are the first WELD land cover change data sets for the CONUS and are available for download at the official WELD website (ftp://weldftp.cr.usgs.gov/CONUS_5Y_LandCover/). Results indicate a capability for national-scale monitoring using turn-key approaches that advance current pathfinding efforts for CONUS (Homer, Huang, Yang, Wylie, & Coan, 2004). Analyses from the forest cover change results reveal a highly varied national-scale forest change dynamic, with the southeastern U.S. the most disturbed region and the northeastern U.S. the least. Core forests absent of change were identified and LiDAR data employed to quantify forest height differences in the spectral/spatial delineation of core forests. Given the lack of a wall-to-wall spaceborne LiDAR capability, integrated uses of this kind will be required to maximize the utility of available LiDAR data. The direct use of disturbance data will be useful to future assessments of forest integrity (Potapov et al., 2008) and fragmentation (Heilman, Strittholt, Slosser, & Dellasala, 2002). Bare ground was related to urbanization through a comparison with census data that proved to be viable for cities outside of desert or semi-desert environments. However, the majority of bare ground gain was found outside of metropolitan areas in the form of mining, transportation infrastructure and natural causes.

The validation exercise highlighted product limitations, some of which can be addressed by improving training data, creating a more robust image feature space and modifying definition sets to account for differences in temporal and spatial observational scales. Lengthening the study period will improve the discrimination of land cover conversion versus more ephemeral transitional cover states. Land cover classifications have legends related to structural–physiognomic vegetation

Fig. 16. Example validation blocks for bare ground gain. Left to right are 1) reference GoogleEarth™ validation time 1 imagery, 2) time 2 imagery, 3) bare ground gain over Landsat reference image where gray is bare ground gain agreement, red is WELD bare ground gain and magenta is validation bare ground gain, and 4) visual confusion matrix where dark gray equals bare ground gain agreement, light gray no bare ground gain agreement, red commission error and magenta omission error.

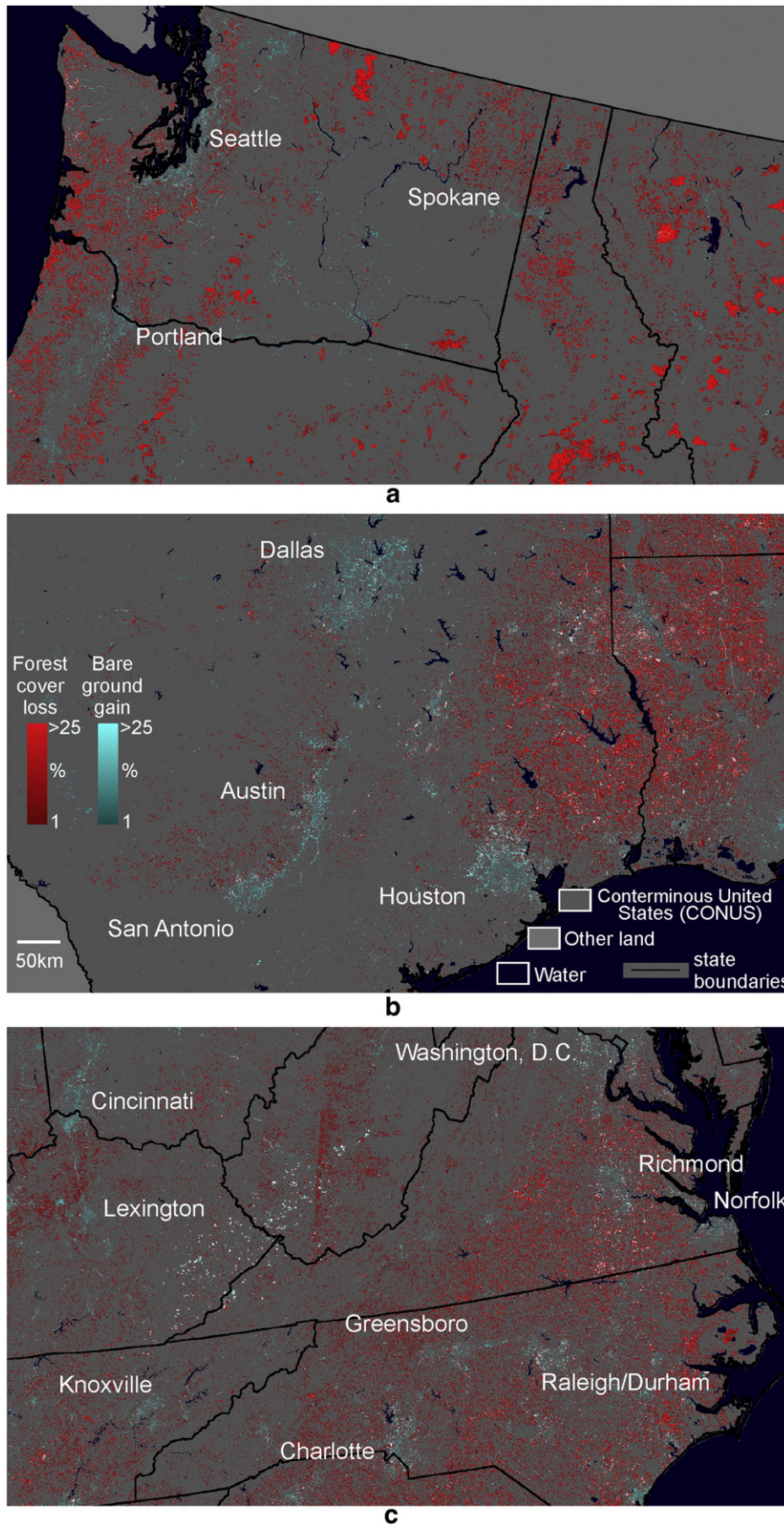


Fig. 17. Regional subsets of 920 km by 560 km centered on a) the northwest, b) east Texas, and c) the Mid-Atlantic, with major cities indicated.

traits (DiGregorio & Jansen, 1998) and similar definition sets are needed for land cover change classes, including temporal considerations. For example, monthly, annual and decadal bare ground gain each represents very different land change dynamics. The addition of contemporaneous Landsat 5 data would provide more cloud-free surface observations than Landsat 7 data alone and has been suggested for improved global land cover mapping (Kovalsky & Roy, 2013).

Questions regarding the appropriate scale (regional/national/continental/global) to apply single characterization models remain. While it may be assumed that more accurate products are made possible by stratifying on ecoregions, or other pre-determined sub-areas, this has not been definitively proven. The use of validation data to assess such approaches is recommended. In this manner, an evidence-based protocol to implementing large area land cover characterizations can be employed. Despite this, the initial use of WELD data presented here shows promise for future operational implementations of large area land change monitoring. The long-term data continuity, robust calibration, systematic acquisition strategy, free data policy, and ready access of Landsat data assure its preeminence in national to global scale land monitoring efforts. Next steps will include the development of prototype global-scale products in support of the GEO global land cover initiative.

References

- Breiman, L. (1996). Bagging predictors. *Machine Learning*, 24, 123–140.
- Breiman, L., Friedman, J. H., Olshen, R. A., & Stone, C. J. (1984). *Classification and regression trees*. Monterey, California: Wadsworth and Brooks/Cole.
- Broich, M., Hansen, M. C., Potapov, P., Adusei, B., Lindquist, E., & Stehman, S. V. (2011). Time-series analysis of multi-resolution optical imagery for quantifying forest cover loss in Sumatra and Kalimantan, Indonesia. *International Journal of Applied Earth Observation and Geoinformation*, 13, 277–291.
- Caccetta, P. A., Furby, S. L., O'Connell, J., Wallace, J. F., & Wu, X. (June 25–29). Continental monitoring: 34 years of land cover change using Landsat imagery. *32nd International Symposium on Remote Sensing of Environment* (San José, Costa Rica).
- Chander, G., Markham, B.L., & Helder, D. L. (2009). Summary of current radiometric calibration coefficients for Landsat MSS, TM, ETM₊, and EO-1 AUI sensors. *Remote Sensing of Environment*, 113, 893–903.
- Chang, J., Hansen, M. C., Pittman, K., Dimiceli, C., & Carroll, M. (2007). Corn and soybean mapping in the United States using MODIS time-series data sets. *Agronomy Journal*, 1654–1664.
- Collins, B. J., Rhoades, C. C., Underhill, J., & Hubbard, R. M. (2010). Post-harvest seedling recruitment following mountain pine beetle infestation of Colorado lodgepole pine stands: a comparison using historic survey records. *Canadian Journal of Forestry Research*, 40, 2452–2456.
- DeFries, R., Hansen, M., & Townshend, J. (1995). Global discrimination of land cover types from metrics derived from AVHRR Pathfinder data. *Remote Sensing of Environment*, 54, 209–222.
- DeFries, R., Hansen, M., Steining, M., Dubayah, R., Sohlberg, R., & Townshend, J. (1997). Subpixel forest cover in Central Africa from multisensor, multitemporal data. *Remote Sensing of Environment*, 60, 228–246.
- DeFries, R., Hansen, M., Townshend, J. R. G., & Sohlberg, R. (1998). Global land cover classifications at 8 km spatial resolution: The use of training data derived from Landsat imagery in decision tree classifiers. *International Journal of Remote Sensing*, 19, 3141–3168.
- Department of the Interior (2010). United States launches new global initiative to track changes in land cover and use. Washington, DC: Department of the Interior News Release November 5, 2010. www.doi.gov/news/pressreleases/United-States-Launches-New-Global-Initiative-to-Track-Changes-in-Land-Cover-and-Use-Data-Sharing-Will-Assist-Land-Managers-Worldwide.cfm
- DiGregorio, A., & Jansen, L. J. M. (1998). *Land Cover Classification System (LCCS): Classification concepts and user manual*. Rome: Food and Agricultural Organization.
- Drummond, M.A., & Loveland, T. R. (2010). Land-use pressure and a transition to forest-cover loss in the Eastern United States. *Bioscience*, 60, 286–298.
- Friedl, M.A., & Brodley, C. E. (1997). Decision tree classification of land cover from remotely sensed data. *Remote Sensing of Environment*, 61, 399–409.
- Friedl, M.A., McIver, D. K., Hodges, J. C. F., Zhang, X. Y., Muchoney, D., Strahler, A. H., et al. (2002). Global land cover mapping from MODIS: Algorithms and early results. *Remote Sensing of Environment*, 83, 287–302.
- Gao, B. (1996). NDWI — A normalized difference water index for remote sensing of vegetation liquid water from space. *Remote Sensing of Environment*, 58, 257–266.
- Ghimire, B., Rogan, J., Panday, P., Neeti, N., & Galiano, V. (2012). An evaluation of bagging, boosting, and random forest for land-cover classification of Cape Cod, Massachusetts, USA. *GIScience and Remote Sensing*, 49, 623–643.
- Goetz, S. J., & Dubayah, R. O. (2011). Advances in remote sensing technology and implications for measuring and monitoring forest carbon stocks and change. *Carbon Management*, 2, 231–244.
- Goetz, S. J., Sun, M., Baccini, A., & Beck, P.S. A. (2010). Synergistic use of space-borne LiDAR and optical imagery for assessing forest disturbance: An Alaska case study. *Journal of Geophysical Research - Biogeosciences*, 115, G00E07. <http://dx.doi.org/10.1029/2008JG000898>.
- Goetz, S. J., Wright, R. K., Smith, A. J., Zinecker, E., & Schaub, E. (2003). IKONOS imagery for resource management: Tree cover, impervious surfaces, and riparian buffer analyses in the mid-Atlantic region. *Remote Sensing of Environment*, 88(1–2), 195–208.
- Gong, P., Wang, J., Yu, L., Zhao, Y., Liang, L., Niu, Z., et al. (2013). Finer resolution observation and monitoring of global land cover: first mapping results with Landsat TM and ETM+ data. *International Journal of Remote Sensing*, 34, 2607–2654.
- Hansen, M. (2012). *Classification trees and mixed pixel training data, chap. 9 of Giri, C.P., remote sensing of land use and land cover—Principles and applications*. Boca Raton, FL: CRC Press, 127–136 (Also available online at <http://dx.doi.org/10.1201/b11964-3>)
- Hansen, M. C., DeFries, R. S., Townshend, J. R. G., Carroll, M., Dimiceli, C., & Sohlberg, R. A. (2003). Global percent tree cover at a spatial resolution of 500 meters: First results of the MODIS vegetation continuous fields algorithm. *Earth Interactions*, 7(10) (15 pp. [online journal]).
- Hansen, M. C., & DeFries, R. S. (2004). Detecting long term global forest change using continuous fields of tree cover maps from 8 km AVHRR data for the years 1982–1999. *Ecosystems*, 7, 695–716.
- Hansen, M., Dubayah, R., & DeFries, R. (1996). Classification trees: An alternative to traditional land cover classifiers. *International Journal of Remote Sensing*, 17, 1075–1081.
- Hansen, M. C., Egorov, A., Roy, D. P., Potapov, P., Ju, J., Turubanova, S., et al. (2011). Continuous fields of land cover for the continuous United States using Landsat data: First results from the Web-Enabled Landsat Data (WELD) project. *Remote Sensing Letters*, 2(4), 279–288.
- Hansen, M. C., Stehman, S. V., & Potapov, P. V. (2010). Quantification of global gross forest cover loss. *Proceedings of the National Academy of Sciences*, 107, 8650–8655.
- Hansen, M. C., Stehman, S. V., Potapov, P. V., Loveland, T. R., Townshend, J. R. G., DeFries, R. S., et al. (2008). Humid tropical forest clearing from 2000 to 2005 quantified using multi-temporal and multi-resolution remotely sensed data. *Proceedings of the National Academy of Sciences*, 105, 9439–9444.
- Hansen, M. C., Townshend, J. R. G., DeFries, R. S., & Carroll, M. (2005). Estimation of tree cover using MODIS data at global, continental and regional/local scales. *International Journal of Remote Sensing*, 26, 4359–4380.
- Harper, G. J., Steining, M. K., Tucker, C. J., Juhn, D., & Hawkins, F. (2007). Fifty years of deforestation and forest fragmentation in Madagascar. *Environmental Conservation*, 34, 1–9.
- Heilman, G. E., Strittholt, J. R., Slosser, N. C., & Dellasala, D. A. (2002). Forest fragmentation of the Conterminous United States: Assessing forest intactness through road density and spatial characteristics. *Bioscience*, 52, 411–422.
- Holben, B. (1986). Characteristics of maximum-value composite images from temporal AVHRR data. *International Journal of Remote Sensing*, 7, 1417–1434.
- Homer, C., Huang, C., Yang, L., Wylie, B., & Coan, M. (2004). Development of a 2001 national land-cover database for the United States. *Photogrammetric Engineering and Remote Sensing*, 70, 829–840.
- Huang, C., Goward, S., Masek, J., Gao, F., Vermote, E., Thomas, N., et al. (2009). Development of time series stacks of Landsat images for reconstructing forest disturbance history. *International Journal of Digital Earth*, 2, 195–218.
- Hudak, A. T., Lefsky, M.A., Cohen, W. B., & Berterretche, M. (2002). Integration of lidar and Landsat ETM+ data for estimating and mapping forest canopy height. *Remote Sensing of Environment*, 82, 397–416.
- Instituto Nacional de Pesquisas Espaciais (INPE) (2010). Deforestation estimates in the Brazilian Amazon, São José dos Campos: INPE. <http://www.obt.inpe.br/prodes>
- Irons, J. R., & Loveland, T. R. (2013). Eighth Landsat satellite becomes operational. *Photogrammetric Engineering and Remote Sensing*, 79, 398–401.
- Ju, J., & Roy, D. P. (2008). The availability of cloud-free Landsat ETM+ data over the conterminous United States and globally. *Remote Sensing of Environment*, 112, 1196–1211.
- Kennedy, R. E., Yang, Z., & Cohen, W. B. (2010). Detecting trends in forest disturbance and recovery using yearly Landsat time series: 1. LandTrendr — Temporal segmentation algorithms. *Remote Sensing of Environment*, 114(12), 2897–2910.
- Killeen, T. J., Calderon, V., Soria, L., Quezada, B., Steining, M. K., Harper, G., et al. (2007). Thirty years of land-cover change in Bolivia. *Ambio*, 36, 600–606.
- Kovalsky, V., & Roy, D. P. (2013). The global availability of Landsat 5 TM and Landsat 7 ETM+ land surface observations and implications for global 30 m Landsat data product generation. *Remote Sensing of Environment*, 130, 280–293.
- Lee, D. S., Storey, J. C., Choate, M., & Hayes, R. W. (2004). Four years of Landsat-7 on-orbit geometric calibration and performance. *IEEE Transactions on Geoscience and Remote Sensing*, 42, 2786–2795.
- Leimgruber, P., Kelly, D. S., Steining, M. K., Brunner, J., Muller, T., & Songer, M. (2005). Forest cover change patterns in Myanmar (Burma) 1990–2000. *Environmental Conservation*, 32, 356–364.
- Loveland, T. R., Sohl, T. L., Stehman, S. V., Gallant, A. L., Saylor, K. L., & Napton, D. E. (2002). A strategy for estimating the rates of recent United States land cover changes. *Photogrammetric Engineering and Remote Sensing*, 68, 1091–1099.
- Margono, B.A., Turubanova, S., Zhuravleva, I., Potapov, P., Tyukavina, A., Baccini, A., et al. (2012). Mapping and monitoring deforestation and forest degradation in Sumatra (Indonesia) using Landsat time series data sets from 1990 to 2010. *Environmental Research Letters*, 7. <http://dx.doi.org/10.1088/1748-9326/7/3/034010>.
- Markham, B.L., Storey, J. C., Williams, D. L., & Irons, J. R. (2004). Landsat sensor performance: History and current status. *IEEE Transactions on Geoscience and Remote Sensing*, 42, 2691–2694.
- Masek, J. G., Huang, C., Wolfe, R., Cohen, W., Hall, F., Kutler, J., et al. (2008). North American forest disturbance mapping from a decadal Landsat record. *Remote Sensing of Environment*, 112, 2914–2926.

- Michaelson, J., Schimel, D. S., Friedl, M.A., Davis, F. W., & Dubayah, R. O. (1994). Regression tree analysis of satellite and terrain data to guide vegetation sampling and surveys. *Journal of Vegetation Science*, 5, 673–696.
- Olson, D. M., Dinerstein, E., Wikramanayake, E. D., Burgess, N. D., Powell, G. V. N., Underwood, E. C., et al. (2001). Terrestrial ecoregions of the World: A new map of life on Earth. *Bioscience*, 51, 1–6.
- Potapov, P., Turubanova, S., Zhuravleva, I., Hansen, M., Yaroshenko, A., & Manisha, A. (2012a). Forest cover change within the Russian European North after the breakdown of the Soviet Union (1990–2005). *International Journal of Forestry Research*, 2012, 11 pp. <http://dx.doi.org/10.1155/2012/729614>.
- Potapov, P. V., Turubanova, S. A., Hansen, M. C., Adusei, B., Broich, M., Altstatt, A., et al. (2012b). Quantifying forest cover loss in Democratic Republic of the Congo, 2000–2010, with Landsat ETM+ data. *Remote Sensing of Environment*, 122, 106–116.
- Potapov, P., Yaroshenko, A., Turubanova, S., Dubinin, M., Laestadius, L., Thies, C., et al. (2008). Mapping the world's intact forest landscapes by remote sensing. *Ecology and Society*, 13 (URL: <http://www.ecologyandsociety.org/vol13/iss2/art51/>)
- Reed, B. C., Brown, J. F., VanderZee, D., Loveland, T. R., Merchant, J. W., & Ohlen, D. O. (1994). Measuring phenological variability from satellite imagery. *Journal of Vegetation Science*, 5, 703–714.
- Ripley, B.D. (1996). *Pattern recognition and neural networks*. New York: Cambridge University Press.
- Roy, D. P. (2000). The impact of misregistration upon composited wide field of view satellite data and implications. *IEEE Transactions on Geoscience and Remote Sensing*, 38, 2017–2031.
- Roy, D. P., Ju, J., Kline, K., Scaramuzza, P. L., Kovalskyy, V., Hansen, M., et al. (2010). Web-enabled Landsat Data (WELD): Landsat ETM+ composited mosaics of the conterminous United States. *Remote Sensing of Environment*, 114, 35–49.
- Sexton, J. O., Song, X. -P., Feng, M., Noojipady, P., Anand, A., Huang, C., et al. (2013a). Global, 30-m resolution continuous fields of tree cover: Landsat-based rescaling of MODIS vegetation continuous fields with lidar-based estimates of error. *International Journal of Digital Earth*, 6, 427–448.
- Sexton, J. O., Song, X. -P., Huang, C., Channan, S., Baker, M. E., & Townshend, J. R. (2013b). Urban growth of the Washington, D.C.–Baltimore, MD metropolitan region from 1984 to 2010 by annual, Landsat-based estimates of impervious cover. *Remote Sensing of Environment*, 129, 42–53.
- Syphard, A.D., Radeloff, V. C., Keuler, N. S., Taylor, R. S., Hawbaker, T. J., Stewart, S. I., et al. (2008). Predicting spatial patterns of fire on a southern California landscape. *International Journal of Wildland Fire*, 17, 602–613.
- Townshend, J. R., Masek, J. G., Huang, C., Vermote, E., Gao, F., Channan, S., et al. (2012). Global characterization and monitoring of forest cover using Landsat data: Opportunities and challenges. *International Journal of Digital Earth*, 5, 373–397.
- Wang, C., Lu, Z., & Haithcoat, T. L. (2007). Using Landsat images to detect oak decline in the Mark Twain National Forest, Ozark Highlands. *Forest Ecology and Management*, 240, 70–78.
- Wickham, J. D., Stehman, S. V., Gass, L., Dewitz, J., Fry, J. A., Wade, T. G., et al. (2013). Accuracy assessment of NLCD 2006 land cover and impervious surface. *Remote Sensing of Environment*, 130, 294–304.
- Woodcock, C. E., Allen, R., Anderson, M., Belward, A., Bindschadler, R., Cohen, W., Gao, F., et al. (2008). Free access to Landsat imagery. *Science*, 320, 1011.
- Wulder, M.A., Masek, J. G., Cohen, W. B., Loveland, T. R., & Woodcock, C. E. (2012). Opening the archive: How free data has enabled the science and monitoring promise of Landsat. *Remote Sensing of Environment*, 122, 2–10.
- Xian, G., & Homer, C. (2010). Updating the 2001 National Land Cover Database impervious surface products to 2006 using Landsat imagery change detection methods. *Remote Sensing of Environment*, 114, 1676–1686.
- Xian, G., Homer, C., & Fry, J. (2009). Updating the 2001 National Land Cover Database land cover classification to 2006 by using Landsat imagery change detection methods. *Remote Sensing of Environment*, 113, 1133–1147.
- Zhu, Z., Woodcock, C. E., & Olofsson, P. (2013). Continuous monitoring of forest disturbance using all available Landsat imagery. *Remote Sensing of Environment*, 122, 75–91.